Marine Micropaleontology 182 (2023) 102258

Contents lists available at ScienceDirect

Marine Micropaleontology

journal homepage: www.elsevier.com/locate/marmicro

To be or not to be a conodont. The controversial story of *Pseudooneotodus* and *Eurytholia*

Annalisa Ferretti [a], Carlo Corradini [b], Sana Fakir [a], Daniele Malferrari [a,*], Luca Medici [c]

[a] Department of Chemical and Geological Sciences, University of Modena and Reggio Emilia, Via Campi 103, 41125 Modena, Italy
[b] Department of Mathematics and Geosciences, University of Trieste, Via Weiss 2, 34128 Trieste, Italy
[c] National Research Council of Italy, Institute of Methodologies for Environmental Analysis, C. da S. Loja-Zona Industriale, 85050 Tito Scalo, Potenza, Italy

ARTICLE INFO

Keywords:
Bioapatite
Microstructure
HFSE
SEM-FIB
X-ray microdiffraction and FWHM
Conodonts

ABSTRACT

The genus *Pseudooneotodus* (Drygant, 1974) is a genus of small and conical elements widely distributed from the Middle Ordovician to the Early Devonian throughout the world. Because of its unusual shape, *Pseudooneotodus* has long been considered enigmatic, and only in the late nineties of the last century the genus has been finally placed within conodonts according to histological data.

This study investigates possible similarities between *Pseudooneotodus* and *Eurytholia* (Sutton et al., 2001), an *incertae sedis* genus of enigmatic plates with a phosphate composition. An association of over one hundred specimens of *Pseudooneotodus beckmanni* and *Eurytholia bohemica* was analyzed from conodont residues in two distinct geographical areas: the Prague Basin (Požáry and Mušlovka sections, Bohemia, Czech Republic) and the Carnic Alps (Rauchkofel Boden section, Austria). Through an investigation that combines the use of optical and electron microscopy (including focused ion beam scanning electron microscopy), X-ray microdiffraction, and trace element (HFSE) analysis by mass spectrometry, differences between these fossil groups were observed and compared with data resulting from typical conodonts (*Dapsilodus obliquicostatus*, *Panderodus unicostatus* and *Wurmiella excavata*) recovered from the same samples.

1. Introduction

The taxonomic affinity of conodonts has been a matter of long and animated discussion among specialists. The recovery of the first conodont animals with preserved soft parts in the last decades of the previous century has allowed the assignment of conodonts to vertebrates by most conodont workers (see a summary in Ferretti et al., 2020, but with possible alternative views in Blieck et al., 2010 and Turner et al., 2010). However, a phosphatic composition is not exclusive to conodonts, and the attribution of bioapatite material extracted from acid digested residues to conodonts is not automatic, unless the existence of a counterpart documented in conodont natural assemblages or the recovery of conodont clusters. This is especially true if the morphology of the specimen is somehow diverse from the typical conodont element shape of a main cusp possibly bearing long denticulated processes.

Pseudooneotodus (Drygant, 1974) is a genus with extensive worldwide distribution ranging from the Middle Ordovician to the Early Devonian and having a peculiar small and conical shape, recalling the Ordovician genus *Oneotodus* Lindström (so the name *Pseudooneotodus*; Corradini, 2008). Because of its unusual morphology, *Pseudooneotodus* had long been considered not to be a conodont, and various hypotheses on its biological affinity were advanced. Möstler (1968) referred to the skeletal elements of the genus as "pseudoconodonts", Serpagli (1970) considered them to be "problematic", Flügel and Schönlaub (1972) regarded them as fish teeth, and Winder (1976) suggested possible similarities with gastropods and bryozoans. Other authors, however, identified morphological similarities with conodonts. Jentzsch (1962) noticed that the growth lamellae are overlapping in the basal cavity and Schulze (1968) compared the basal filling of *Pseudooneotodus* with that of conodonts. Drygant (1974) finally assigned these elements to conodonts, and Barrick (1977) confirmed the "conodont hypothesis" on the basis of the "same colour, luster and type of the basal material as found in undoubted conodonts from the same remains" (p. 57), proposing as well a first apparatus architecture. Sansom (1996) conducted a histological study on *Pseudoonetodus*, finally confirming the attribution of *Pseudooneotodus* to conodonts.

Pseudooneotodus is documented from the Darriwilian (Middle Ordovician, *Histiodella holodentata* Zone; Stouge, 1984) to the Emsian (Early

* Corresponding author.
E-mail address: daniele.malferrari@unimore.it (D. Malferrari).

https://doi.org/10.1016/j.marmicro.2023.102258
Received 22 April 2023; Received in revised form 2 June 2023; Accepted 9 June 2023
Available online 13 June 2023

Devonian; Schulze, 1968). A total of eight species and one subspecies are known: *Pseudooneotodus mitratus* (Moskalenko), *P. mitrectus* (Moskalenko), *P. nostras* (Moskalenko), *P. humilis* Orchard in the Ordovician; *P. tricornis* Drygant, *P. bicornis bicornis* Drygant, *P. bicornis contiguus* Corradini, *P. linguicornis* Jeppsson and *P. beckmanni* (Bischoff and Sannemann) in the Silurian; the latter is the only species documented in the Early Devonian (Corradini, 2008).

The genus *Eurytholia* was introduced by Sutton et al. (2001) to describe small "hat-like" phosphatic sclerites of unknown origin found in residues of samples prepared for conodont analysis from the Middle to Upper Ordovician of some sectors bordering the Iapetus Ocean (South Wales, UK; Alabama, USA; Dalarna, Sweden; and North Estonia). The millimetre-sized plates had a typical "cap" shape with a raised upper zone and were assigned to two species of *Eurytholia* (*E. prattensis* Sutton, Holmer and Cherns, and *E. elibata* Sutton, Holmer and Cherns). The elements of *Eurytholia* were interpreted as dorsal dermal sclerites of a problematic animal, ovoid in shape, bearing sub-longitudinal rows of sclerites (Sutton et al., 2001).

Similar sclerites, ranging from 0.3 mm to 2 mm, were recovered from Silurian and Lower Devonian conodont residues in several sections of the Czech Republic (Butovice, Kosov Quarry, Amerika Quarry, Mušlovka Quarry, Požáry, and U Topolů) and attributed to the new species *Eurytholia bohemica* (Ferretti et al., 2006). *Eurytholia bohemica* differs from the Ordovician species described by Sutton et al. (2001) by the presence of a well-developed girdle with an inner groove running along the margin of the plates. According to the authors, this belt might have facilitated the anchoring of the sclerite in a more rigid outer layer. In addition, some of the stratigraphically younger specimens found in the Koněprusy area lacking the belt and having distinctly concave side walls could have represented another species, but the material was insufficient for a firm taxonomic assessment. A small association of *Eurytholia bohemica* was later described (Ferretti and Serpagli, 2008) in the upper Silurian of the Carnic Alps from a single sample (level 326) from the Rauchkofel Boden section. Recently, the species was reported from the Silurian of Sardinia (Corradini et al., 2009), the Silurian of Ireland (Ferretti et al., 2021a; Kaminski et al., 2016) and the Lochkovian of Sardinia (Corriga et al., 2022).

Mergl (2019) recently described *Eurytholia* from Middle Devonian conodont residues from Central Bohemia (Czech Republic). Given the paucity of material found, the new specimens were identified as *Eurytholia* aff. *bohemica*. Based on the similarity in morphology and histology, as well as the perfect overlap of stratigraphical range, Mergl (2019) highlighted the relationship of *Pseudooneotodus* and *Eurytholia*, suggesting that *Eurytholia* could belong as well to vertebrates.

As mentioned above, one feature common to all the organisms under study is the phosphatic (bioapatite) composition. Bioapatite is a material of strictly biochemical origin that is broadly assigned the general formula $Ca_5(PO_4,CO_3)_3(F,OH)$ (Keenan et al., 2015; Skinner, 2005). Various iso- and hetero-valent substitutions may occur in anionic and cationic sites either during *in-vivo* biologically-mediated crystal growth or in *post-mortem* burial and diagenesis (Zapanta LeGeros, 1981). Calcium may be substituted by major elements (*e.g.*, Brigatti et al., 2004; Keenan and Engel, 2017) or by REE (Rare Earth Elements) and other HFSE (High-Field-Strength Elements, *e.g.*, Grandjean-Lécuyer et al., 1993; Li et al., 2017; Reynard et al., 1999; Trotter et al., 2007; Trotter and Eggins, 2006; Trueman and Tuross, 2002; Zhao et al., 2013) and the content of trace elements in fossil bioapatite was for a long time assumed as a reliable marker of sea-water composition (*e.g.*, Girard and Albarède, 1996; Grandjean et al., 1987; Grandjean-Lécuyer et al., 1993; Wright et al., 1984). Nevertheless, since about three decades ago (Armstrong et al., 2001; Holser, 1997; Picard et al., 2002; Reynard et al., 1999; Toyoda and Tokonami, 1990), concrete hypotheses have emerged that HFSE concentrations in bioapatite are significantly affected by chemical and mineralogical composition of the diagenetic environment (Chen et al., 2015; Herwartz et al., 2013; Kocsis et al., 2010; Liao et al., 2019; Trotter et al., 2016; Trotter and Eggins, 2006; Zhang et al., 2016; Zhao et al., 2013; Žigaitė et al., 2020) and, as recently proposed (Medici et al., 2021), also by the morphology of the fossil remain, although not in such a way as to distort the diagenetic contribution. Although there is not yet unanimous agreement, the multifactorial diagenetic footprint hypothesis as the major characterizing imprint of HFSE content is the most widely endorsed (Chen et al., 2015; Kim et al., 2012; Lécuyer et al., 2004; Trotter et al., 2016; Zhang et al., 2016). Therefore, bioapatite can be tagged (hydrogen signature) during life (Grandjean-Lécuyer et al., 1993; Lécuyer et al., 2004; Nothdurft et al., 2004; Webb et al., 2009; Webb and Kamber, 2000; Wright et al., 1987), but it is in the burial environment that HFSE uptake is greatly boosted by diagenesis (pore-water signature) (Chen et al., 2015; Pattan et al., 2005; Zhang et al., 2016). A quick assessment of REE sources can be based on the Th *vs* ΣREE and Y/Ho *vs* ΣREE cross-plots (Li et al., 2017). In fact, high ΣREE (sum of all REE content) and strong LREE (light REE, *i.e.*, sum of La and Ce) and Th enrichment characterize the pore-water contribution (McLennan, 2001; Peppe and Reiners, 2007; Shen et al., 2012; Wright and Colling, 1995); on the other hand, high Y/Ho are indicative of an hydrogen signature as, in modern ocean water, Ho is adsorbed or complexed at about twice the rate of Y (Nozaki et al., 1997; Zhang et al., 1994; Zhang and Nozaki, 1996). More difficult is the interpretation of MREE (middle REEs, *i.e.*, sum of Pr, Nd, Sm, Eu) and HREE (heavy REEs, *i.e.*, sum of Gd, Tb, Dy, Ho, Er, Tm, Yb, Lu) enrichments as their contribution could reflect an authigenic phosphate signal (Bright et al., 2009; Reynard et al., 1999; Sholkovitz and Shen, 1995), further complicating the interpretation of the results.

The diagenetic footprint can also be assessed by measuring parameters related to the crystal structure of the bioapatite, although this approach is rarely used and has sometimes led to questionable results (Ferretti et al., 2017; Medici et al., 2021; Pucéat et al., 2004; Trueman et al., 2008; Trueman and Tuross, 2002; Žigaitė et al., 2020). These parameters include, for example, bioapatite cell volume and crystallinity index; the correlation with diagenesis is that the higher (and longer) the pressure and temperature to which a crystal is exposed, the higher the resulting crystallinity index and the smaller the cell volume (Ferretti et al., 2021b; Medici et al., 2021). As will be better detailed in the Results section, an additional feature that is closely related to crystallinity and on which the crystallinity index value also depends, is the Full Width at Half Maximum (FWHM) of selected diffraction peaks. In fact, the FWHM is a parameter that can be directly correlated with both crystal grain distortion and structural disorder (Kim and Chung, 2003; Tung et al., 2009); in other words, a linear increase in the FWHM of a diffraction peak denotes both a deformation of individual crystals and increased disorder in the bioapatite lattice which, in turn, can be related to the diagenetic imprint.

Following the indication of Mergl (2019), specimens of *Pseudooneotodus* and *Eurytholia* recovered from the same conodont residues and of the same age throughout the samples were compared through the application of a survey protocol on bioapatite crystal-chemistry and trace element composition (Ferretti et al., 2021b; Ferretti et al., 2017; Malferrari et al., 2019; Medici et al., 2020; Medici et al., 2021), complemented by the use of focused ion beam scanning electron microscopy, applied to conodonts following the pioneer investigations by Rosseeva et al. (2011) and Zhuravlev and Gerasimova (2015). The study was extended to undoubted conodonts ("true" conodonts: *Dapsilodus obliquicostatus* (Branson and Mehl), *Panderodus unicostatus* (Branson and Mehl) and *Wurmiella excavata* (Branson and Mehl)) recovered from the same samples producing *Pseudooneotodus* and *Eurytholia* in order to minimize the number of uncontrollable variables.

The purpose of the work is to test whether the diagenetic signature completely masked the life-print information and whether additional evidence can help in refining the taxonomic assignment of both *Pseudooneotodus* and *Eurytholia*.

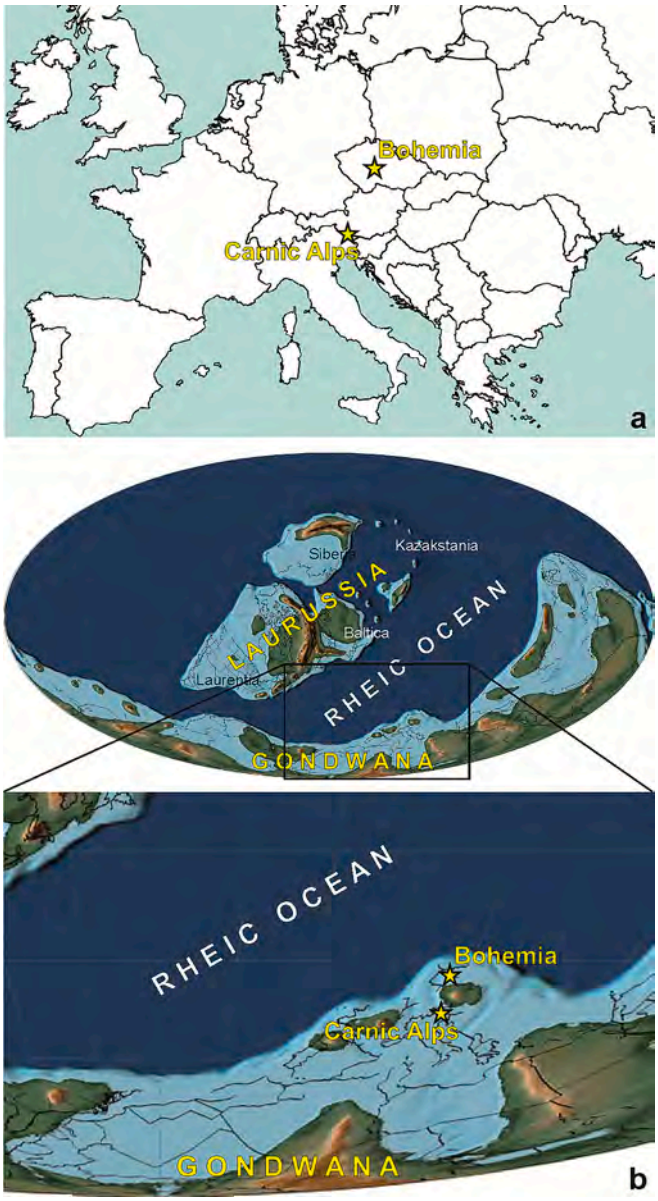

Fig. 1. (a) Overview map with modern location of the study sites in Bohemia and the Carnic Alps. (b) Paleogeographical reconstruction of the late Silurian (modified after Scotese, 2014). Yellow stars indicate location of the two investigated areas. (For interpretation of the references to colour in this figure legend, the reader is referred to the web version of this article.)

2. Geological setting

The study material comes from the Silurian of Bohemia and the Carnic Alps (Fig. 1a). During the lower Paleozoic these areas belong to a group of terranes (Fig. 1b) that detached from the northern Gondwana margin during the Ordovician and drifted northward faster that the main continent. Beside Bohemia and the Carnic Alps, these terrains include Sardinia, the Montagne Noire and the Pyrenees, among others, and are known as Galatian Terranes assemblage (von Raumer and Stampfli, 2008). During the late Silurian these terranes were located at mid latitudes in the southern hemisphere (Ferretti et al., 2022; Ferretti et al., 2009; Schönlaub, 1997). Even if their mutual position is still debated, likely Bohemia occupied a slightly northern position than the Carnic Alps (Fig. 1b). However, at first approximation the upper Silurian sequences of the Carnic Alps and Bohemia are similar, being mainly composed by black graptolitic shales and limestones rich in cephalopods.

2.1. Bohemia

In Bohemia lower Paleozoic units are mainly exposed in the Prague Synform, a complex structure formed during the Variscan Orogeny, exposed in the western part of the Czech Republic (Fig. 1a). The marine sedimentary succession of the Prague Synform spans from the Ordovician to the Middle Devonian (Chlupáč et al., 1998). The Silurian rocks are preserved within the core of the synform between Praha and Beroun. Here, the lowermost Silurian rocks are represented by black graptolitic shales, while carbonate deposition increased progressively already starting from the Sheinwoodian (Kříž, 1998), and resulting in the more widespread rock of Přídolí age (Slavík and Hladil, 2017). Volcanic activity developed from several volcanic centers along synsedimenary faults during the Aeronian and from the Sheinwoodian to the Gorstian (Kříž, 1992; Kříž et al., 2003). The study material belongs to the Kopanina Fm. exposed in the Požáry and Mušlovka quarries.

The Kopanina Fm. mainly consists of tuffaceous shales and bioclastic limestone in the lower part and thick cephalopod limestone in the upper part (Ferretti and Kříž, 1995; Kříž et al., 1986; Manda et al., 2023). The transition with the overlying Požáry Fm. is defined by the onset of platy limestones alternated with shales (Kříž, 1998) and appears to be diachronous from the upper Ludlow to the lower Přídolí (Čáp et al., 2003; Kříž et al., 1986; Manda and Kříž, 2006). For detailed description of the Požáry section refer to Kříž (1992), Kříž et al. (1986), Lehnert et al. (2007) and Slavík (2017); for Mušlovka quarry refer to Kříž et al. (1986).

2.2. Carnic Alps

One of the world's most complete and best-exposed Paleozoic successions from the ?Cambrian-Lower Ordovician to the Upper Permian is found in the Carnic Alps (Fig. 1a; Ferretti et al., 2023). For a complete description of this sequence, updated to the recent lithostratigraphical scheme, refer to Corradini et al. (2016, 2015) and Corradini and Pondrelli (2021).

Silurian outcrops are irregularly distributed in the Carnic Alps, and are mainly represented by cephalopod-bearing and shallow-water bioclastic limestones, limestones interbedded with shales, black graptolitic shales and cherts. The overall thickness of Silurian rocks does not exceed 60 m. Although the whole Silurian is documented, a large hiatus above the Upper Ordovician rocks is recorded in some places as a result of Hirnantian glaciation, and various sediment piles are missing up to the Gorstian (Corriga et al., 2021).

Three calcareous formations follow each other in the proximal part of the basin: the Kok Fm. (Telychian-lower Ludfordian), the Cardiola Fm. (Ludfordian) and the Alticola Fm. (Ludfordian-Lochkovian). The material in study was collected from the lowermost bed of the Alticola Fm. exposed in the Rauchkofel Boden section (Schönlaub et al., 2017 and references therein). The Alticola Fm. consists of well bedded grey and pink cephalopod limestones with rare interbedded layers of greyish bioclastic limestones and grey shales (Ferretti et al., 2015; Ferretti et al., 2012). The unit is rich of fossils, represented by orthoceratid cephalopods, bivalves, brachiopods, trilobites, crinoids, and chitinozoans, among others. The age of the unit was precisely defined thanks to the rich conodont fauna (*e.g.*, Corradini et al., 2020; Corradini et al., 2019; Corradini et al., 2015; Corriga et al., 2016; Schönlaub et al., 2017; Walliser, 1964).

3. Materials and methods

3.1. Analyzed material

The material analyzed in this study was selected in order to fulfill a list of premises. A first choice was to investigate long-spanning and geographically widespread taxa. *Pseudooneotodus beckmanni* is by far the

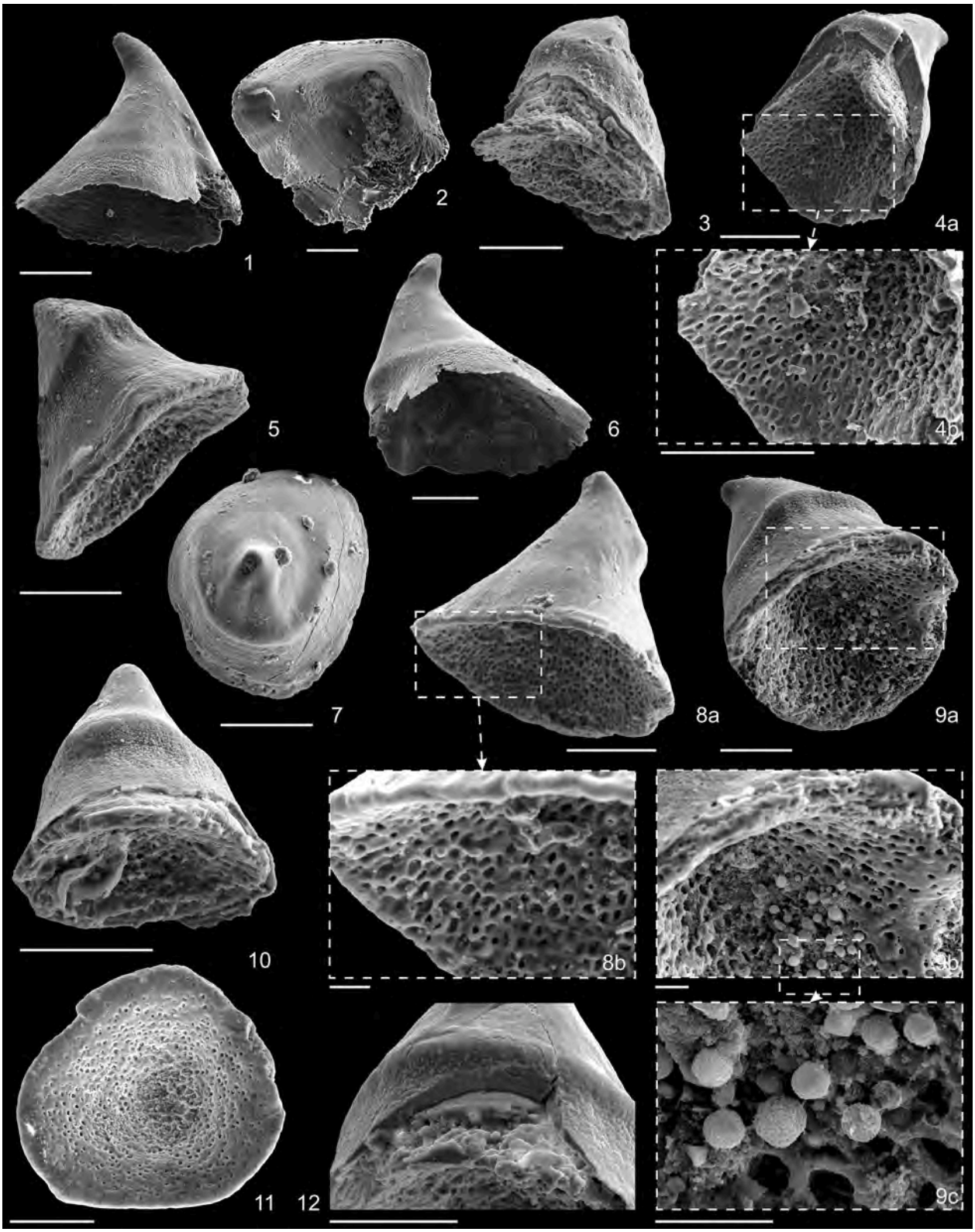

Fig. 2. SEM micrographs of *Pseudooneotodus beckmanni* (Bischoff and Sannemann, 1958). Ludlow, *Polygnathoides siluricus* Zone.
1–2, 6. 1, lateral view of specimen 42, IPUM 35015; 2, lower view of specimen 39, IPUM 35016; 6, lateral view of specimen 41, IPUM 35020; Carnic Alps, sample Rauchkofel Boden 326. The Carnic material exposes the only outer layer of the specimens.
3, 5, 7, 10–11. 3, lower-lateral view of specimen 14, IPUM 35017; 5, lateral view of specimen 9, IPUM 35019; 7, upper view of specimen 8, IPUM 35021; 10, lateral view of specimen 13, IPUM 35024; 11, lower view of specimen 11, IPUM 35025; Bohemia, sample Požáry 1.
4, 8–9, 12. 4a, lower view of specimen 26, IPUM 35018; 4b, detail of the texture of the inner layer of specimen 26; 8a, lower view of specimen 22, IPUM 35022; 8b, detail of the texture of the inner layer of specimen 22; 9a, lower view of specimen 24, IPUM 35023; 9b, detail of the texture of the inner layer of specimen 24; 9c, pyrite framboids; 12, detail of specimen 23 in lateral view, IPUM 35026; Bohemia, sample Mušlovka A. The Bohemian material exposes two layers of the specimens. Scale bar corresponds to 100 μm for all frames except for 8b, 9b and 9c where it corresponds to 20 μm.

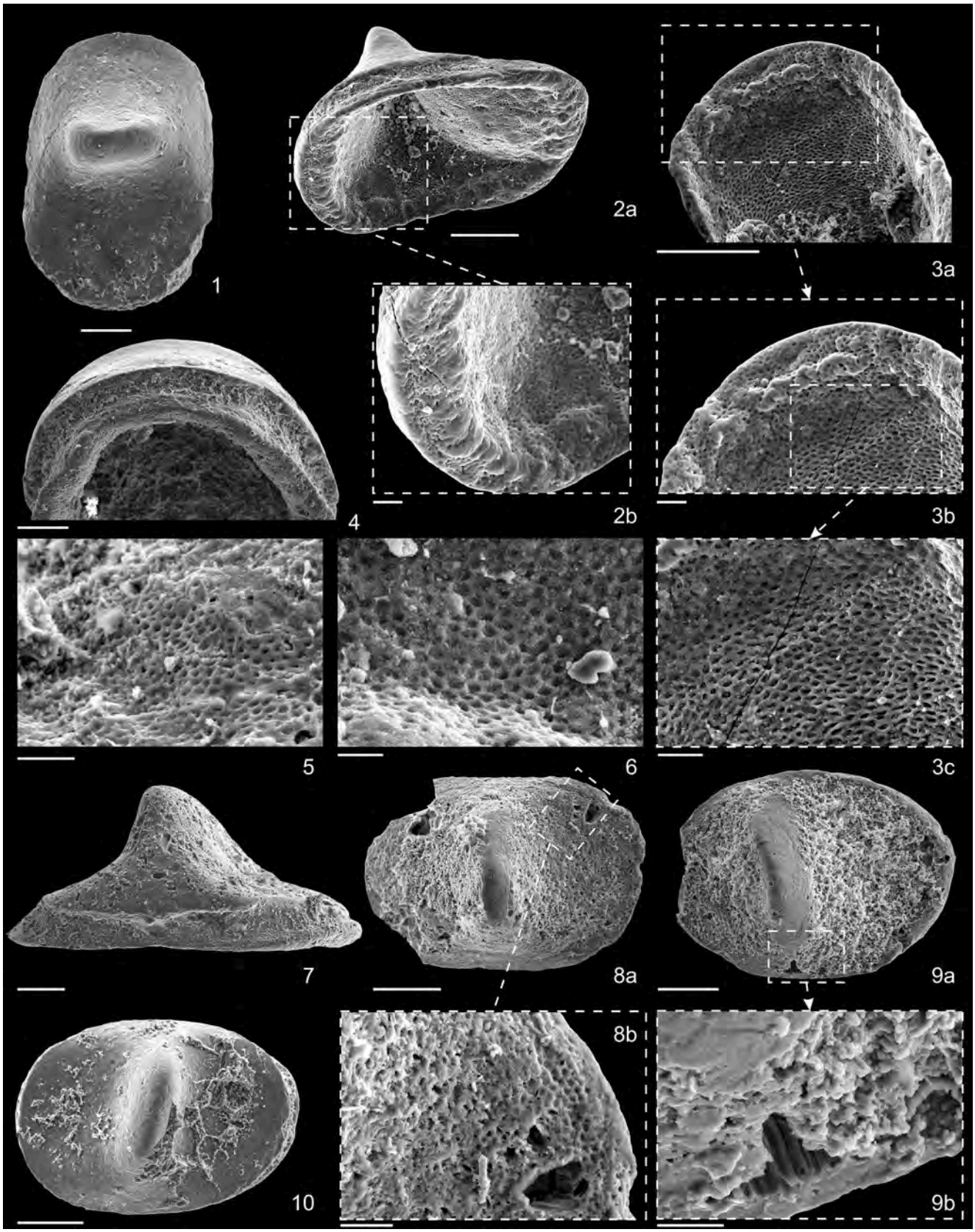

(caption on next page)

Fig. 3. SEM micrographs of *Eurytholia bohemica* Ferretti, Serpagli and Štorch, 2006. Ludlow, *Polygnathoides siluricus* Zone.
1, 3–4, 7. 1, upper view of specimen 1, IPUM 35027; 3a, lower view of specimen 4, IPUM 35029; 3b–3c, details of the inner reticulated layer; 4, lower-lateral view of specimen 5, IPUM 35030, illustrating the typical girdle with an inner groove running along the margin of the specimen; 7, lateral view of specimen 7, IPUM 35033; Bohemia, sample Požáry 1.
2, 6, 10. 2a, lower-lateral view of specimen 15, IPUM 35028; 2b, detail of the inner reticulated layer; 6, detail of the inner reticulated layer of specimen 22, IPUM 35032, in lower view; 10, upper view of specimen 18, IPUM 35036; Bohemia, sample Mušlovka A.
5, 8–9. 5, detail of the inner reticulated layer of specimen 30, IPUM 35031, in lower view; 8a, upper view of specimen 31, IPUM 35034; 8b, detail of the inner reticulated layer exposed by removal of the outer layer; 9a, upper view of specimen 34, IPUM 35035; 9b, detail of the oriented bioapatite crystals of the outer layer; Carnic Alps, sample Rauchkofel Boden 326.
Scale bar corresponds to 100 μm for all frames except for 2b, 3b–3c, 5, 6, 8b and 9b where it corresponds to 20 μm.

most abundant species of the genus, spanning the Silurian and Early Devonian. *Eurytholia bohemica* covers the Silurian up to the Early (and possibly Middle) Devonian. Our selection was therefore restricted to these two taxa. A further choice was to study specimens (*Pseudooneotodus beckmanni*, *Eurytholia bohemica* and "true" conodonts) from exactly the same stratigraphical level; specifically, all our material documents the *Polygnathoides siluricus* conodont Biozone (Ludlow, Silurian). The same age was provided by the Sardinian "Ockerkalk" bearing the association *Eurytholia/Pseudooneotodus* (Corradini et al., 1998; Ferretti et al., 2009; Serpagli et al., 1998). Elements belonging to *Dapsilodus obliquicostatus*, *Panderodus unicostatus* and *Wurmiella excavata* were chosen as "true" conodonts for comparison.

With those premises, three levels were selected, two in Bohemia (Požáry 1 and Mušlovka A) and one in the Carnic Alps (Rauchkofel Boden 326). Samples were treated with an up to 10% solution of formic acid, and the insoluble residue was washed through a 100-μm sieve. Residues were later concentrated, if abundant, with sodium polytungstate.

Resulting material was first investigated under optical microscopy with a Zeiss Stemi SV 11 binocular microscope (magnification 25–100×) in order to select taxa. The most complete specimens with no secondary recrystallization were picked and later deeply characterized.

The illustrated specimens are kept in the Type Collection of the Department of Chemical and Geological Sciences, University of Modena and Reggio Emilia, Modena, Italy under the Repository Numbers IPUM 3501535039.

Under the light microscope, rock samples from the Carnic Alps are composed almost entirely of calcite, mostly microcrystalline or secondary crystallized within fractures or forming phenocrysts of varying sizes. There are also iron oxides and hydroxides, the latter being widespread in the microcrystalline calcite. Chlorite is also occasionally present. Samples from Bohemia, in addition to calcite, document microcrystalline quartz (better identifiable by X-ray diffraction), iron oxides (sometimes with idiomorphic habit and more abundant than in the Carnic Alps) and, rarely, illite; diffraction measurements also indicate the occurrence of dolomite and/or magnesian calcite. Fossil remains are clearly evident from both localities.

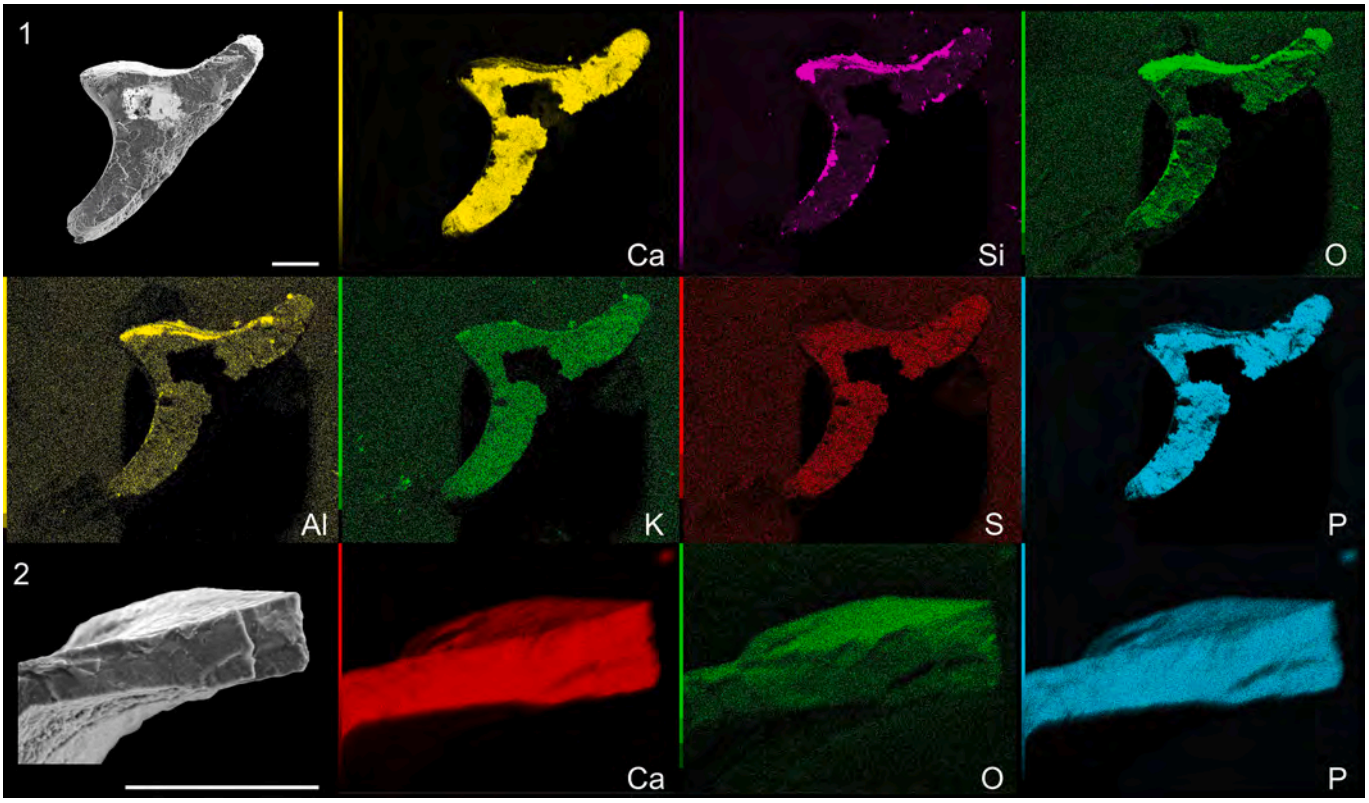

Fig. 4. SEM–EDS elemental maps through broken specimens of *Eurytholia bohemica* and *Pseudooneotodus beckmanni* revealing a general homogeneous composition of the wall. Ludlow, *Polygnathoides siluricus* Zone.
1, Ca, Si, O, Al, K, S and P maps of *Eurytholia bohemica*, specimen 6, IPUM 35037; Bohemia, sample Požáry 1.
2, Ca, O and P maps of *Pseudooneotodus beckmanni*, specimen 35, IPUM 35038; Carnic Alps, sample Rauchkofel Boden 326.
Scale bar corresponds to 100 μm.

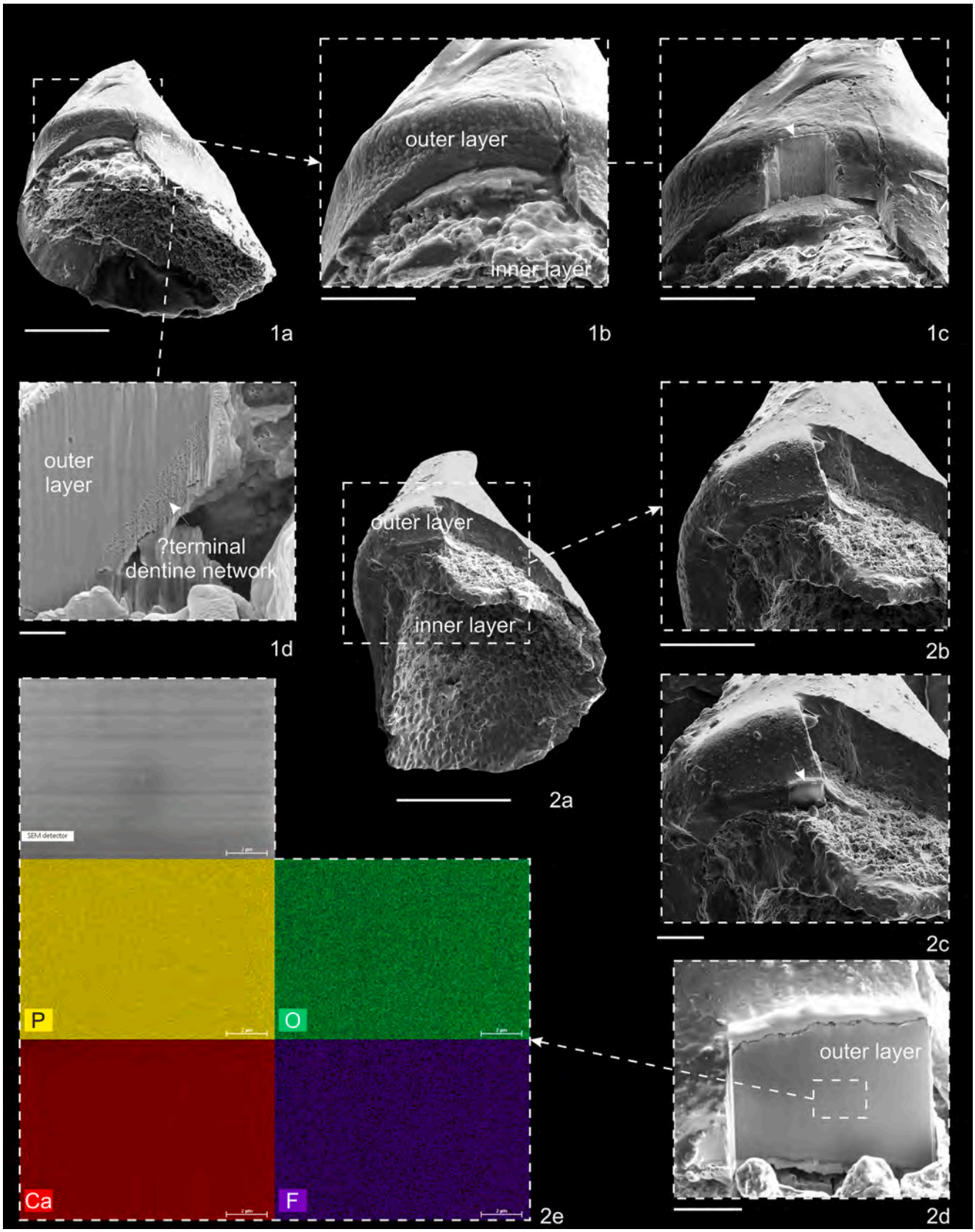

(caption on next page)

Fig. 5. SEM micrographs of *Pseudooneotodus beckmanni* specimens studied under focused ion beam scanning electron microscopy (FIB). Ludlow, *Polygnathoides siluricus* Zone.
1a, lower-lateral view of specimen 23, IPUM 35026; 1b, detail of the inset in 1a clearly exposing the outer and inner layers; 1c, FIB milling of the outer layer (white arrow); 1d, FIB-milled outer layer revealing at the base a porous texture (white arrow) recalling the terminal dentine network of Sansom (1996); Bohemia, sample Mušlovka A.
2a, lower-lateral view of specimen 26, IPUM 35018; 2b, detail of the inset in 2a clearly exposing the outer and inner layers; 2c, FIB milling of the outer layer (white arrow); 2d, FIB-milled outer layer; 2e, SEM–EDS elemental maps (P, O, Ca and F) of the inset in 2d revealing no signification variations in the analyzed spot area; Bohemia, sample Mušlovka A.
Scale bar corresponds to 100 μm for all frames except for 1b–1c and 2 b where it corresponds to 50 μm, for 1d where it corresponds to 2 μm, for 2c where it corresponds to 20 μm and for 2d where it corresponds to 5 μm.

3.2. Instruments and analytical methods

We applied a consolidated multi-analytical protocol (*e.g.*, Malferrari et al., 2019; Medici et al., 2021; Nardelli et al., 2016) for fossil remains characterization encompassing trace elements (HFSE) measurement through laser ablation-inductively coupled plasma mass spectrometry (LA-ICP-MS), X-ray microdiffraction and scanning electron microscopy (SEM) equipped with an energy dispersive X-ray (EDX) detector for major elements quantification. In addition, focused ion beam scanning electron microscopy (SEM-FIB) was used on conodonts in order to polish selected portions of the specimens for further investigation.

As well-known and extensively documented in the literature, the tuning of the experimental parameters, especially those related to LA-ICP-MS, represents a critical issue. To avoid overburdening the text, detailed description of instruments and analytical methods are reported in the Supplementary Online Material (SOM-1).

4. Results

4.1. Morphology and structure

Specimens of *Pseudooneotodus beckmanni* are characterized in lateral view by a short conical shape with a single apical denticle (Figs. 2.1 and 2.6), usually inclined posteriorly, and a rounded (Fig. 2.11) to sub-triangular (Fig. 2.2) basal outline. The external surface is smooth with no visible ornamentation or specific patterns. Some specimens show a marginal girdle, visible in lateral (Figs. 2.5, 2.9a and 2.10) and upper (Fig. 2.7) views, that may expand up to two/thirds of the height of the element (Fig. 2.5). Specimens from the Carnic Alps bear a deep empty basal cavity that occupies the entire lower part of the specimen (Fig. 2.2). On the contrary, material from Bohemia clearly reveals the existence of two separate layers: a thinner outer layer and a thicker inner layer that may occupy part (Figs. 2.4a, 2.8a, 2.9a and 2.11) or most (Figs. 2.3, 2.10 and 2.12) of the basal cavity. The contact between the two layers in broken specimens (Figs. 2.4a, 2.10 and 2.12) is sharp and might possibly have represented an easy surface of detachment of the inner layer. However, in specimens complete of the marginal basal outline (*e.g.*, Figs. 2.8 and 2.9), the two layers appear strongly fused each other.

The outer layer exposed in sectioned cuts is compact and massive (Figs. 2.4a and 2.12). Remarkably, the inner layer shows a reticulated pattern with oval or sub-polygonal meshes of approximately 5 μm size defined by 2–3 μm rods. Peculiar concentrations of pyrite framboids were observed in a few specimens either from Bohemia (*e.g.*, Fig. 2.9c) and the Carnic Alps.

Specimens of *Eurytholia bohemica* have an elliptical shape with linear (Fig. 3.1 and 3.8a) or slightly curved (Fig. 3.9a and 3.10) margins and a median to sub median ridge. The diagnostic well-defined girdle with an inner furrow expands along the basal margin as exposed in lower (Figs. 3.2a and 3.4) and lateral (Fig. 3.7) views. A deep empty basal cavity expands to the apex of the ridge (Fig. 2a).

Eurytholia specimens bear of a compact outer layer and a porous inner layer (Ferretti et al., 2006). The outer wall is made by crystals that are oriented perpendicular to the wall (Fig. 3.9b). The inner layer shows a peculiar reticulated pattern with oval to pseudo-hexagonal meshes (Figs. 3c, 3.5 and 3.6) of approximately 3 μm size with 2 μm rods. The inner layer strictly merges with the outer one along the basal margin (Figs. 3.2b and 3.8b).

4.2. Chemical composition (major elements)

Environmental scanning electron microscopy coupled with micro-analyses (SEM-EDX) was applied to specimens of *Pseudooneotodus beckmanni* and *Eurytholia bohemica* in order to monitor distribution of major elements along the entire surface of the specimens, with special attention to detect possible differences through the two layers exposed by broken elements. Distribution maps of selected elements (P, Ca, O, K, Si, Al, S) and spectra run along continuous lines did not reveal any significant variations through the element wall of both *Eurytholia* (Fig. 4.1) and *Pseudooneotodus* (Fig. 4.2) or along their outer surface.

4.3. Microstructure

Focused ion beams (FIB) have been applied since the 1960s to characterize inorganic and biological materials at the micro- or nano-scales (Lešer et al., 2010). FIB technique offers the opportunity of consuming only a small volume of material and of sectioning exactly the sample at the specific site of interest. Resulting surfaces may be later analyzed with other investigative approaches (see SOM-1 for further details). Selected samples of *Pseudooneotodus beckmanni* and *Eurytholia bohemica* were transferred into FIB/SEM for FIB milling; FIB-milled regions were secondary electron imaged and analyzed by EDX to provide basic compositional data.

Specimens of *Pseudooneotodus beckmanni* with well recognizable inner and outer layers (Figs. 5.1a and 5.2a) were tested in order to select the best spots to be sectioned. FIB-milled outer layer of the specimens revealed a general homogeneity in microstructure and composition for main elements (P, O, Ca and F; Fig. 5.2e), but a porous microtexture emerged in the basal part of the outer layer at the contact with the inner layer (Fig. 5.1d), recalling the terminal dentine network described by Sansom (1996). No micropattern was revealed in the inner layer. A first specimen of *Eurytholia bohemica* was FIB sectioned in the median ridge (Fig. 6.1), in order to expose the outer layer. A second specimen was prepared in order to offer both the inner and outer layer to the focused ion beams (Fig. 6.2c). The outer layer of both investigated specimens revealed a faint lamination (Figs. 6.1f and 6.2d), while no micropattern was detected in the inner layer (Fig. 6.2e).

4.4. HFSE signature

A list of statistically significant relationships among the HFSEs of the investigated material from both Bohemia and the Carnic Alps is given in Supplementary Online Material (SOM-2). All specimens, regardless of taxa and source area, are characterized by a substantial enrichment of MREE and, in part, HREE (Fig. 7), although this behavior appears more pronounced in *Eurytholia* and, to a lesser extent, in *Pseudooneotodus* rather than in "true" conodonts. This trend is also evidenced by the linear distribution of Y with respect to La, Nd and Yb (Fig. 8) considered as representative of LREE, MREE and HREE, respectively, and by the cross-plot of HRRE/LREE *vs* MREE/MREE* (Fig. 9).

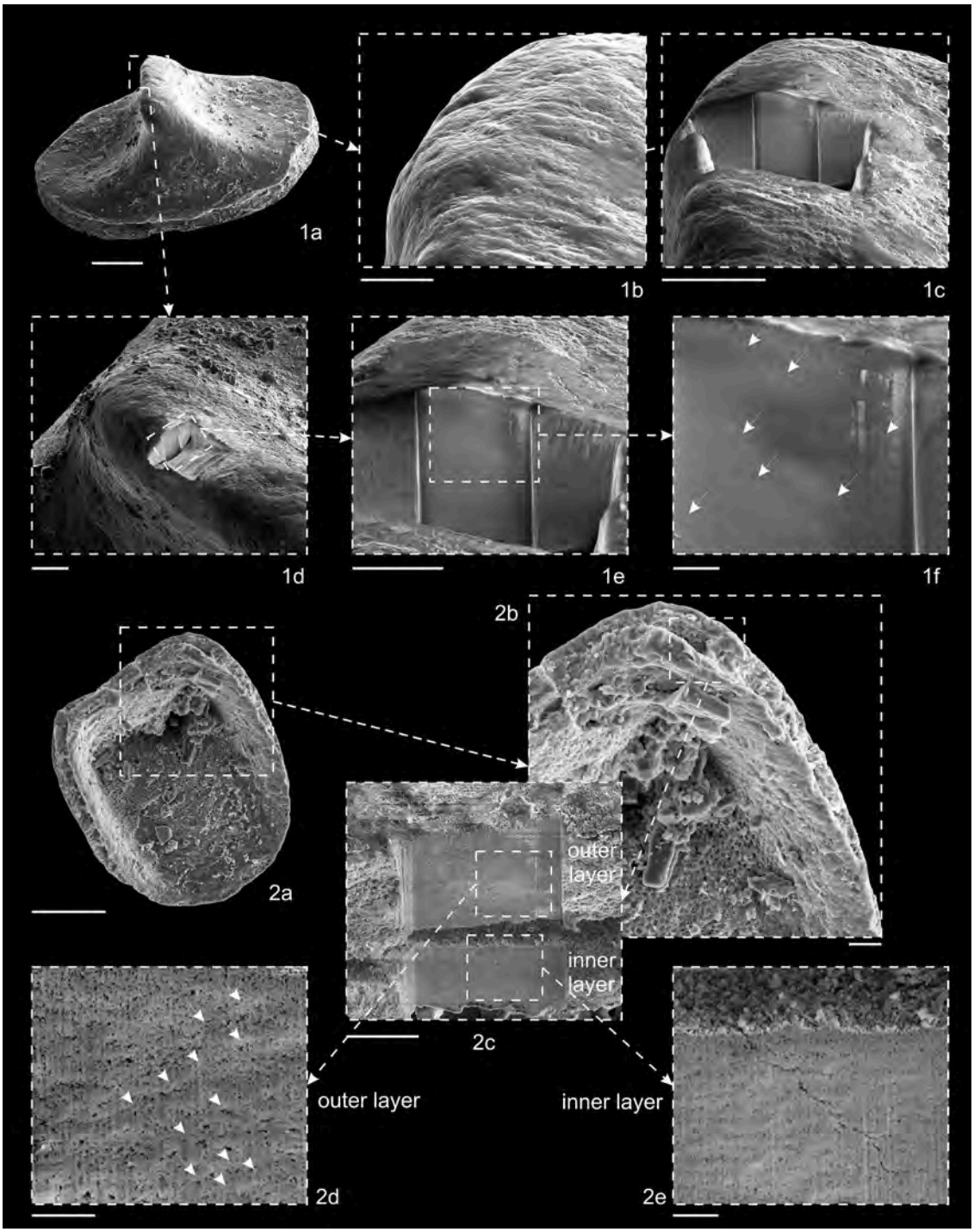

Fig. 6. SEM micrographs of *Eurytholia bohemica* specimens studied under focused ion beam scanning electron microscopy. Ludlow, *Polygnathoides siluricus* Zone.
1a, upper-lateral view of specimen 22, IPUM 35032; 1b, detail of the inset in 1a showing the area of the median ridge planned to be exposed to FIB; 1c-1e, FIB milling of the median ridge so to expose the outer layer; 1f, FIB-milled outer layer revealing a laminated texture (white arrows); Bohemia, sample Mušlovka A.
2a, lower view of specimen 43, IPUM 35039; 2b, detail of the inset in 2a showing the outer and inner layers; 2c, FIB-milled outer and inner layers; 2d, FIB-milled outer layer revealing a faint lamination (white arrows); 2e, FIB-milled inner layer revealing a homogeneous texture; Bohemia, sample Mušlovka A.
Scale bar corresponds to 100 μm for all frames except for 1b–1d and 2b where it corresponds to 20 μm, for 1e and 2c where it corresponds to 10 μm and for 1f, 2d and 2e where it corresponds to 2 μm.

The Y/Ho ratio is particularly useful for distinguishing marine *vs* lithogenic REE sources. In fact, Y and Ho have similar ionic radii and show an analogous vertical distribution profile in modern oceans (Zhang et al., 1994); nevertheless, as mentioned in the Introduction, Ho in waters is removed (adsorbed onto suspended particulate matter or bound by complexants) twice as fast as Y (Bau, 1996; Nozaki et al., 1997; Zhang and Nozaki, 1996). For this reason, the lithogenic sources of REE are characterized by relatively uniform and low Y/Ho ratios, usually between 20 and 30, while seawater shows much higher values, mostly ranging between 60 and 70 (Kamber and Webb, 2001; McLennan, 2001). Since diagenesis results in a general increase in the sum of REE, an increasing value of ΣREE, eventually normalized with respect to Th,

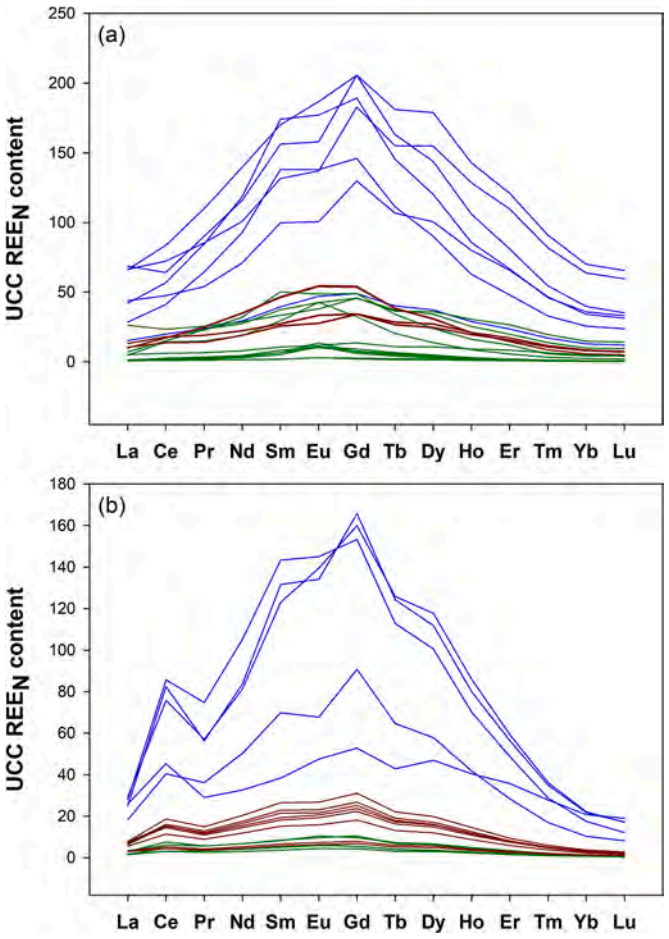

Fig. 7. Upper continental crust (UCC) normalized (McLennan, 2001) REE abundance patterns for *Eurytholia* (blue lines), "true" conodonts (green lines) and *Pseudooneotodus* (dark red lines) from Bohemia (a) and the Carnic Alps (b). (For interpretation of the references to colour in this figure legend, the reader is referred to the web version of this article.)

should be associated with a low Y/Ho ratio indicating that the diagenetic addition of REEs is related to their release from lithogenic material. Data reported in SOM-2 and the plot of ΣREE/Th *vs* Y/Ho (Fig. 10) provide evidence of two perceptibly distinct REE components, having the Carnic material slightly lower values of the Y/Ho ratio compared to the Bohemian one. The cross-plot of log [ΣREE] *vs* Th (Fig. 11) better refines this distinction, further indicating that *Eurytholia* specimens, regardless of provenance, are generally characterized by higher ΣREE values compared to *Pseudooneotodus* and to "true" conodonts, due essentially to the enrichment of MREE. However, the most significant feature evidenced by log [ΣREE] *vs* Th cross-plot (Fig. 11) is the different clustering of *Eurytholia* and *Pseudooneotodus*, with the former concentrated in the right part of the diagram (*i.e.*, low ΣREE content) and the latter in the middle part (medium to high ΣREE). "True" conodonts span from the left to the middle part of the figure (*i.e.*, mostly high REE signature), only partially overlapping data of *Pseudooneotodus*.

Among REE, Ce is an exception since it can also be oxidized with formation of Ce(IV) species that are poorly soluble or easily adsorbed on suspended particulate matter (Sholkovitz and Shen, 1995). This eventuality leads to a negative Ce anomaly (*i.e.*, Ce/Ce* <1.0) in seawater, which can also be enhanced by the alkaline pH that, generally, negatively affects solubility (de Baar et al., 1988; Liu et al., 1988). On the other hand, in anoxic environments, Ce(III) behaves similarly to the other REEs, resulting in little or no inter-element fractionation and a weak or nonexistent Ce anomaly (*i.e.*, Ce/Ce* ~1.0). On this ground, the type and magnitude of Ce anomaly have often been assumed as a valid paleoenvironmental indicator (see Zhang and Shields, 2022 for a recent review). Nevertheless, to better assess the Ce anomaly and to identify whether the anomaly is only apparent (*i.e.*, due to an excess of adjacent REEs), the Pr/Pr* *vs* Ce/Ce* cross-plots, where $Pr/Pr^* = 2Pr_N/(Ce_N + Nd_N)$ and $Ce/Ce^* = 3Ce_N/(2La_N + Nd_N)$, are commonly used (Bau and Dulski, 1996; Chen et al., 2015; Kowal-Linka et al., 2014; Zhang et al., 2016). The results shown in Fig. 12 clearly show positive Ce anomaly for the material from the Carnic Alps, and no anomalies or, at most, slight negative Ce anomalies for the material from Bohemia.

4.5. Crystallinity signature

An additional path that can be tracked to assess the diagenetic footprint is through the bioapatite crystallinity analysis. In better preserved material from the sole Carnic Alps we calculated the FWHM of the X-ray diffraction peaks of the (300) and (002) reflections, which are closely related to the bioapatite cell parameters *a* and *c*, respectively. More specifically, we plotted the ratio $FWHM_{(300)}/FWHM_{(002)}$ *vs* bioapatite cell volume (Fig. 13). Resulting data clearly indicate the occurrence of an inverse correlation regardless of the three main fossil groups investigated. The *c vs a* cross-plot (Fig. 14), a tool already used in past researches (Ferretti et al., 2017; Medici et al., 2021) to highlight isomorphic substitutions, shows a different clustering of "true" conodonts with respect to *Eurytholia/Pseudooneotodus*, being "true" conodonts clustered in the right part of the diagram at higher values of the cell parameter *a*, while *Eurytholia* and *Pseudooneotodus* cluster (and overlap) in the same left-middle part of the diagram (low to medium value of the cell parameter *a*).

5. Discussion

Pseudooneotodus and *Eurytholia* share undoubtedly numerous characteristics. Both have a conical, cap-like shape, with great variability in the apical part and a wide variation in outline, with a hollow basal part and two distinct layers with externally flared basal margins. The outer layer of both *Pseudooneotodus* and *Eurytholia* appears compact and massive, with a porous microtexture in the basal part of *Pseudooneotodus* and a faint lamination in *Eurytholia* revealed by FIB analysis. The inner layer shows a reticulated pattern with oval or sub-polygonal meshes in both *Pseudooneotodus* and *Eurytholia* of comparable size. The origin of HFSE embedded in fossil remains is not easily circumscribed. However, normalized distributions of REE, REE anomalies, and correlation between REE and/or other trace elements are widely used for reconstructing palaeoceanographic conditions. On the other hand, several evidences also confirm that the REE signature is greatly affected by diagenesis. In our samples, diagenesis undoubtedly leads to an increase in total REE content and, particularly, in MREE (Fig. 7). A flat distribution of REE may develop as a result of organic matter degradation (Kim et al., 2012) in contrast, the bulge determined by MREE enrichment, although often documented in the literature (*e.g.*, Bright et al., 2009; Grandjean et al., 1987; Grandjean-Lécuyer et al., 1993; Kidder et al., 2003; Lécuyer et al., 2004; Zhao et al., 2013) is not yet explained with certainty. One of the most accepted hypotheses (Haley et al., 2004) relates it to the precipitation and dissolution processes of iron oxides and hydroxides, which, because of their high surface charge and colloidal character, may strongly bind cations. A further hypothesis considers the selective adsorption of LREE and HREE by Mn and Fe oxides, respectively, leaving the residual content (MREE) in pore waters (Prakash et al., 2012; Soyol-Erdene and Huh, 2013). However, the observation that MREE enrichment discriminates *Eurytholia* from the other taxa ("true" conodonts, and *Pseudooneotodus*) raises several questions, especially since all specimens realistically underwent identical diagenetic imprinting having been collected from the same sample. The reasons for this differentiation could be attributable to specimen morphology or to original imprinting (in a broad sense). Relative to the former, hypotheses had already been made in the past (Medici et al., 2021), pointing

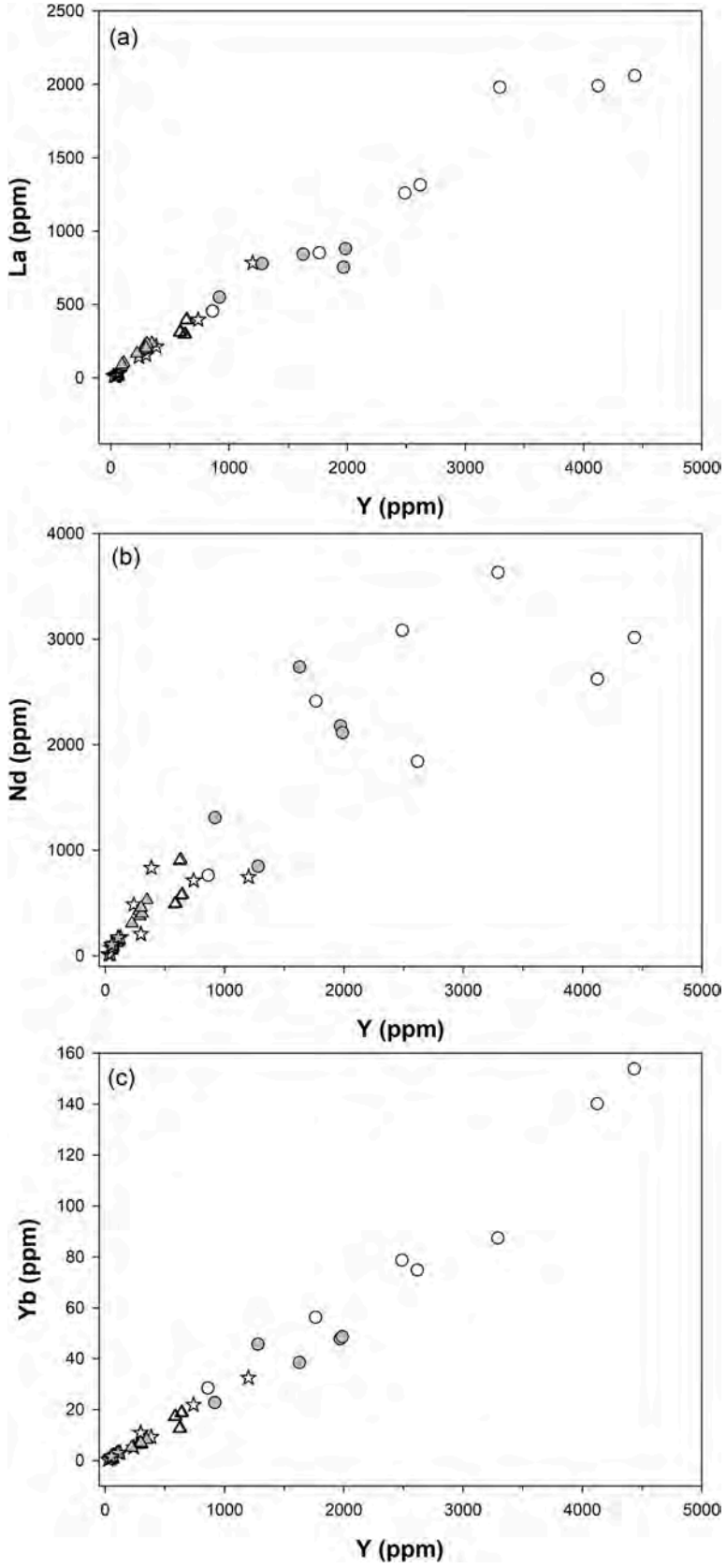

Fig. 8. Cross-plots La (a), Nd (b) and Yb (c) *vs* Y. Legend: "true" conodonts (stars), *Eurytholia* (circles) and *Pseudooneotodus* (triangles); open symbols are used for the Bohemian material, filled symbols for the Carnic one.

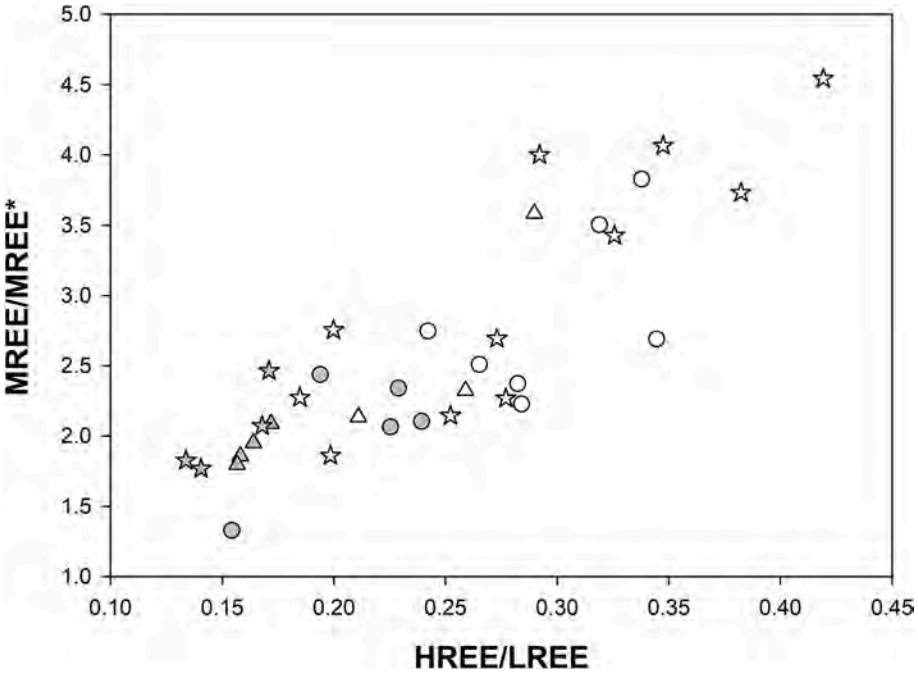

Fig. 9. Cross-plots of MREE/MREE* *vs* HREE/LREE. Symbols like in Fig. 8.

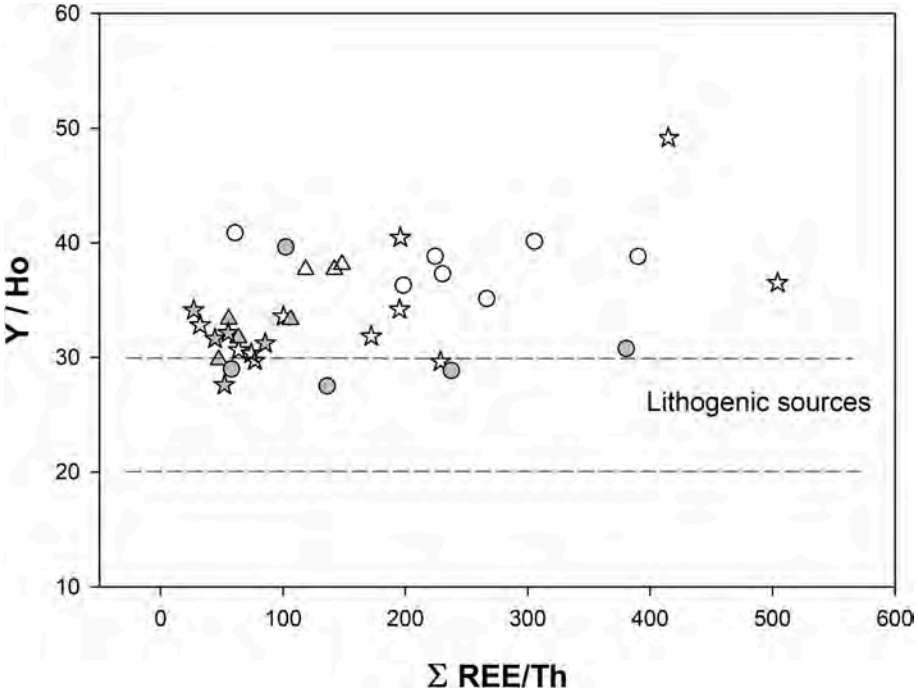

Fig. 10. Cross-plots of Y/Ho *vs* ΣREE/Th. Symbols like in Fig. 8. The field between dashed lines is representative of lithogenic sources.

out that the degree of chemical fractionation depends not only on the effective diffusion coefficient but also on the size of the exposed surface, a parameter, the latter, that has always been assumed to be negligible.

The presence of two perceptibly distinct REE components marked by the ΣREE/Th *vs* Y/Ho trend (Fig. 10) provides evidence that, although the detrital component should be considered as prevalent for both investigated areas (Bohemia and the Carnic Alps), the presence of a slight persistence of the hydrogen signature should not be ruled out for the samples from Bohemia. The cross-plot of log [ΣREE] *vs* Th (Fig. 11), which better refines this distinction, further indicates that *Eurytholia*, regardless of provenance, is generally characterized by high ΣREE values compared to *Pseudooneotodus* and "true" conodonts. In fact, low ΣREE and Th values indicate non-detrital derivation, whereas higher ΣREE but lower ΣREE/Th reflect the faster uptake of Th than REE during diagenesis. This aspect is confirmed for "true" conodonts also by the Y/Ho ratio (mean values ~34 and 31 for Bohemia and the Carnic Alps, respectively), highlighting the contribution of the diagenetic fingerprint along with the mild persistence of the hydrogen signature.

The positive Ce anomaly for the Carnic material suggests that the (*ante* diagenesis) marine and/or pore waters were controlled by

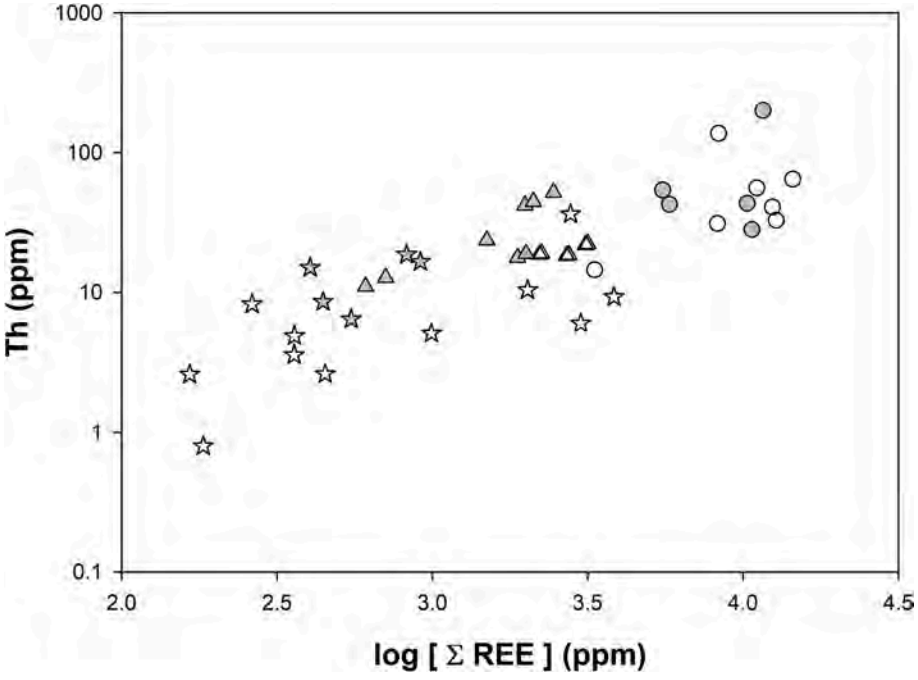

Fig. 11. Cross-plots of Th *vs* log [ΣREE]. Symbols like in Fig. 8.

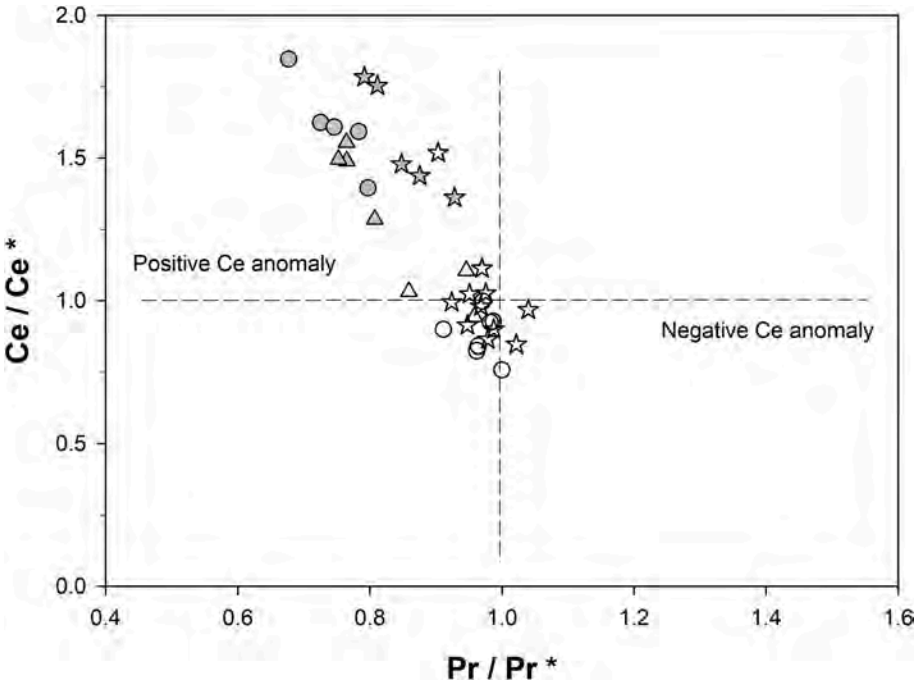

Fig. 12. Location of the studied samples in the McLennan (2001) normalized plots of (Ce/Ce*) *vs* (Pr/Pr*) labelled as $(Ce/Ce^*)_N$ and $(Pr/Pr^*)_N$, respectively. Adapted from Kowal-Linka et al. (2014). Symbols like in Fig. 8.

oxygenated seawater during life and/or early stages of fossilization; however, the presence of pyrite framboids (observed in *Pseudooneotodus* from both the Carnic Alps and Bohemia) indicates the establishment of possible local and temporary reducing conditions. In addition to Ce, Eu is also a redox-sensitive REE that, in strongly reducing environments, can be reduced to Eu(II) creating a possible fractionation with respect to other REEs (Elderfield, 1988). Nevertheless, this transformation affects magmatic rather than sedimentary environments and, in the latter, positive Eu anomalies (*i.e.*, Eu/Eu* >1.0) are more an indication of REE contributions from plagioclase-rich sediments (where Eu replaces Ca) rather than from femic phases, which are commonly associated with negative anomalies (Taylor and McLennan, 1985). However, this differentiation is not well reflected in our material (Fig. 12b), which shows Eu anomaly varying from strongly positive to neutral for "true" conodonts (predominantly Bohemian ones) and from neutral to negative for all other specimens.

The existing inverse correlation between bioapatite cell volume and the $FWHM_{(300)}/FWHM_{(002)}$ ratio (Fig. 13) indicates that the fossilization process involves the increase of carbon content in the lattice of bioapatite with a consequent decrease of both the cell volume and the

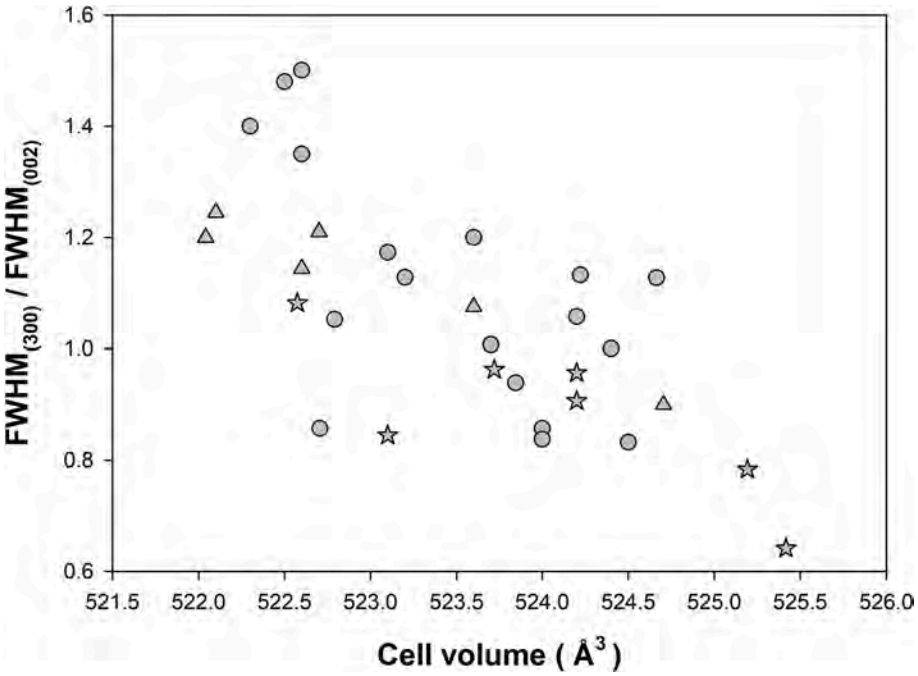

Fig. 13. Inverse correlation between $FWHM_{(300)}/FWHM_{(002)}$ and bioapatite cell volume for samples from the Carnic Alps. Symbols like in Fig. 8.

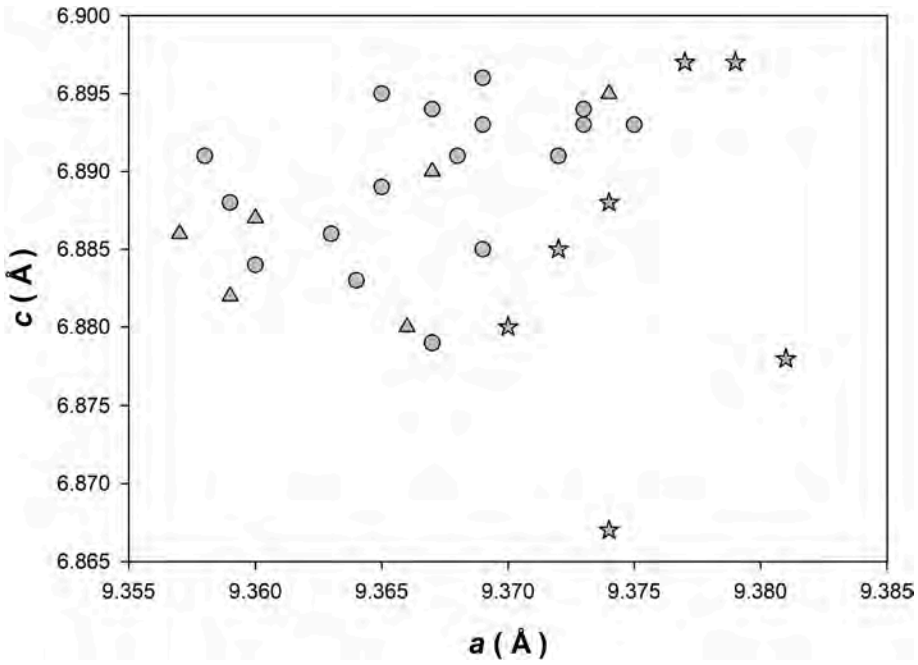

Fig. 14. Distinct clustering of "true" conodonts with respect to *Pseudoonetodus/Eurytholia* evidenced by the bioapatite *c vs a* correlation. Symbols like in Fig. 8.

crystallinity according to the orientation of *a* parameter. These new data confirm that bioapatite cell volume generally decreases with time and, specifically for very ancient (Paleozoic) fossils, bioapatite volume falls in the range of 525 ± 3 $Å^3$ (Ferretti et al., 2021b).

The different clustering of "true" conodonts with respect to *Eurytholia* and *Pseudooneotodus* evidenced by the cross-plot *c vs a* (Fig. 14), even if for now only detected from the Carnic Alps, is in agreement with the HFSE distribution (Figs. 7 and 11, SOM-2). In fact, a high REE and Th content is indicative of a higher diagenetic footprint, while higher values of the cell parameter *a* in "true" conodonts indicate a lower influence of diagenesis (Ferretti et al., 2021b). The greater effectiveness of the diagenetic imprinting in *Eurytholia* could also be confirmed by the presence in the outer layer of crystals that are oriented perpendicularly to the wall itself (Fig. 3.9b). However, even in this circumstance, the crystallinity does not allow to verify whether the original chemical imprint is indeed still present, although, at least for "true" conodonts, it seems to point in that direction.

6. Conclusion

The specimens analyzed in this study are undoubtedly characterized by a nonnegligible diagenetic signature, however, with small but significant distinctions among taxa that predominantly differentiate *Eurytholia* from conodonts and *Pseudooneotodus*. Whether these differences

are attributable to a variable diagenetic imprint related to the morphology of the specimen or rather to its taxonomic location and ecological niche in life cannot be determined with certainty; nevertheless, it is significant that similar geochemical differences were found for specimens from different localities. Preliminary results on bioapatite cell parameters, run so far only on material from the Carnic Alps, appear to indicate a different crystallographic signature of *Pseudooneotodus* and *Eurytholia* with respect to "true" conodonts. Further integrated investigation is requested in order to provide a larger data-set so to possibly suggest more precise taxonomic assignments.

Declaration of Competing Interest

The authors declare that they have no known competing financial interests or personal relationships that could have appeared to influence the work reported in this paper.

Data availability

Numerical data are reported in SOM-2

Acknowledgements

Dr. Gian Carlo Gazzadi (S3 Center, Nanoscience Institute – CNR, Modena) kindly assisted in focused ion beam scanning electron microscopy. We are grateful to the Scientific Instruments Facility, CIGS (University of Modena and Reggio Emilia), and especially to Daniela Manzini for LA-ICP-MS expertise.

AF acknowledges UNIMORE grant 2022 "Biomineralizzazioni in fosfato di calcio nel record geologico". This paper is a contribution to IGCP Project n. 652 "Reading geologic time in Paleozoic sedimentary rocks".

Appendix A. Supplementary data

Supplementary data to this article can be found online at https://doi.org/10.1016/j.marmicro.2023.102258.

References

Armstrong, H.A., Pearson, D.G., Griselin, M., 2001. Thermal effects on rare earth element and strontium isotope chemistry in single conodont elements. Geochim. Cosmochim. Acta 65, 435–441. https://doi.org/10.1016/S0016-7037(00)00548-2.

Barrick, J.E., 1977. Multielement simple cone conodonts from the Clarita Formation (Silurian), Arbuckle Mountains, Oklahoma. Geol. Palaeontol. 11, 47–68.

Bau, M., 1996. Controls on the fractionation of isovalent trace elements in magmatic and aqueous systems: evidence from Y/Ho, Zr/Hf, and lanthanide tetrad effect. Contrib. Mineral. Petrol. 123, 323–333. https://doi.org/10.1007/s004100050159.

Bau, M., Dulski, P., 1996. Distribution of yttrium and rare-earth elements in the Penge and Kuruman iron-formations, Transvaal Supergroup, South Africa. Precambrian Res. 79, 37–55. https://doi.org/10.1016/0301-9268(95)00087-9.

Blieck, A., Turner, S., Burrow, C.J., Schultze, H.-P., Rexroad, C.B., Bultynck, P., Nowlan, G.S., 2010. Fossils, histology, and phylogeny: why conodonts are not vertebrates. Episodes 33, 234–241. https://doi.org/10.18814/epiiugs/2010/v33i4/002.

Brigatti, M.F., Malferrari, D., Medici, L., Ottolini, L., Poppi, L., 2004. Crystal chemistry of apatites from the Tapira carbonatite complex. Brazil. Eur. J. Mineral. 16, 677–685. https://doi.org/10.1127/0935-1221/2004/0016-0677.

Bright, C.A., Cruse, A.M., Lyons, T.W., MacLeod, K.G., Glascock, M.D., Ethington, R.L., 2009. Seawater rare-earth element patterns preserved in apatite of Pennsylvanian conodonts? Geochim. Cosmochim. Acta 73, 1609–1624. https://doi.org/10.1016/j.gca.2008.12.014.

Čáp, P., Vacek, F., Vorel, T., 2003. Microfacies analysis of Silurian and Devonian type sections (Barrandian, Czech Republic). Czech Geol. Surv. Spec. Pap. 15, 40.

Chen, J., Algeo, T.J., Zhao, L., Chen, Z.-Q., Cao, L., Zhang, L., Li, Y., 2015. Diagenetic uptake of rare earth elements by bioapatite, with an example from Lower Triassic conodonts of South China. Earth-Sci. Rev. 149, 181–202. https://doi.org/10.1016/j.earscirev.2015.01.013.

Chlupáč, I., Havlíček, V., Kříž, J., Kukal, Z., Štorch, P., 1998. Palaeozoic of the Barrandian (Cambrian to Devonian). Český geologický ústav, Praha.

Corradini, C., 2008. The conodont Genus *Pseudooneotodus* Drygant from the Silurian and Lower Devonian of Sardinia and the Carnic Alps (Italy). Boll. Soc. Paleontol. Ital. 46, 139–148.

Corradini, C., Pondrelli, M., 2021. The pre-Variscan sequence of the Carnic Alps (Italy-Austria). Geol. Field Trips Maps 13, 1–72. https://doi.org/10.3301/GFT.2021.05.

Corradini, C., Ferretti, A., Serpagli, E., Barca, S., 1998. The Ludlow-Pridoli section Genna Ciuerciu, west of Silius. Gior. Geologia 60, 112–118.

Corradini, C., Ferretti, A., Corriga, M.G., Serpagli, E., 2009. The reference section of the Sardinian Ockerkalk: the Silius Section. Rend. Soc. Paleont. It. 3, 209–216.

Corradini, C., Corriga, M.G., Männik, P., Schönlaub, H.P., 2015. Revised conodont stratigraphy of the Cellon section (Silurian, Carnic Alps). Lethaia 48, 56–71. https://doi.org/10.1111/let.12087.

Corradini, C., Pondrelli, M., Simonetto, L., 2016. Stratigraphy of the La Valute area (Mt. Zermula massif, Carnic Alps, Italy). Boll. Soc. Paleontol. Ital. 55–78 https://doi.org/10.4435/BSPI.2016.06.

Corradini, C., Corriga, M.G., Pondrelli, M., Serventi, P., Simonetto, L., Ferretti, A., 2019. Lochkovian (Lower Devonian) marine-deposits from the Rio Malinfier West section (Carnic Alps, Italy). Ital. J. Geosci. 138, 153–170. https://doi.org/10.3301/IJG.2018.33.

Corradini, C., Corriga, M.G., Pondrelli, M., Suttner, T.J., 2020. Conodonts across the Silurian/Devonian boundary in the Carnic Alps (Austria and Italy). Palaeogeogr. Palaeoclimatol. Palaeoecol. 549, 109097 https://doi.org/10.1016/j.palaeo.2019.02.023.

Corriga, M.G., Floris, M., Corradini, C., 2022. The Silurian/Lower Devonian sequence at Perda S'altari (SW Sardinia, Italy). Boll. Soc. Paleontol. Ital. 61, 71–86. https://doi.org/10.4435/BSPI.2022.02.

Corriga, M.G., Corradini, C., Schönlaub, H.P., Pondrelli, M., 2016. Lower Lochkovian (Lower Devonian) conodonts from Cellon section (Carnic Alps, Austria). Bull. Geosci. 261–270 https://doi.org/10.3140/bull.geosci.1594.

Corriga, M.G., Corradini, C., Pondrelli, M., Schönlaub, H.-P., Nozzi, L., Todesco, R., Ferretti, A., 2021. Uppermost Ordovician to lowermost Devonian conodonts from the Valentintörl section and comments on the post Hirnantian hiatus in the Carnic Alps. Newsl. Stratigr. 54, 183–207. https://doi.org/10.1127/nos/2020/0614.

de Baar, H.J.W., German, C.R., Elderfield, H., van Gaans, P., 1988. Rare earth element distributions in anoxic waters of the Cariaco Trench. Geochim. Cosmochim. Acta 52, 1203–1219. https://doi.org/10.1016/0016-7037(88)90275-X.

Drygant, D., 1974. Prostye konodonty silura i nizov devona Volyno- Podol'ya [simple conodonts from the Silurian and lowermost Devonian of Volyno-Podolia]. Palaeontol. Sb. 10, 64–70.

Elderfield, H., 1988. The oceanic chemistry of the rare-earth elements. Philos. Trans. R. Soc. Lond. Ser. Math. Phys. Sci. 325, 105–126. https://doi.org/10.1098/rsta.1988.0046.

Ferretti, A., Serpagli, E., 2008. *Eurytholia* plates (Problematica) from the late Silurian of the Austrian Carnic Alps. Rev. Micropaleontol. 51 https://doi.org/10.1016/j.revmic.2006.11.002.

Ferretti, A., Serpagli, E., Štorch, P., 2006. Problematic phosphatic plates from the Silurian-Early Devonian of Bohemia, Czech Republic. J. Paleontol. 80, 1026–1031. https://doi.org/10.1666/0022-3360(2006)80[1026:PPPFTS]2.0.CO;2.

Ferretti, A., Corradini, C., Oggiano, G., Štorch, P., 2009. Silurian palaeogeography of northern Gondwana: where was Sardinia at that time? Boll. Soc. Paleontol. Ital. Suppl. 48, 67–76.

Ferretti, A., Cavalazzi, B., Barbieri, R., Westall, F., Foucher, F., Todesco, R., 2012. From black-and-white to colour in the Silurian. Palaeogeogr. Palaeoclimatol. Palaeoecol. 367–368, 178–192. https://doi.org/10.1016/j.palaeo.2012.10.025.

Ferretti, A., Schönlaub, H.P., Corradini, C., Corriga, M.G., Pondrelli, M., Simonetto, L., Serventi, P., 2015. Alticola Formation. In: Corradini, C., Suttner, T.J. (Eds.), The Pre-Variscan Sequence of the Carnic Alps (Austria and Italy), Jb. Geol. B.-A., vol. 69, pp. 56–60.

Ferretti, A., Kříž, J., 1995. Cephalopod Limestone Biofacies in the Silurian of the Prague Basin. Bohemia. PALAIOS 10, 240. https://doi.org/10.2307/3515255.

Ferretti, A., Malferrari, D., Medici, L., Savioli, M., 2017. Diagenesis does not invent anything new: Precise replication of conodont structures by secondary apatite. Sci. Rep. 7 https://doi.org/10.1038/s41598-017-01694-4.

Ferretti, A., Bancroft, A.M., Repetski, J.E., 2020. GECkO: Global Events impacting COnodont evolution. Palaeogeogr. Palaeoclimatol. Palaeoecol. 549, 109677 https://doi.org/10.1016/j.palaeo.2020.109677.

Ferretti, A., Malferrari, D., Savioli, M., Siepe, T., Medici, L., 2021a. 'Conodont pearls' do not belong to conodonts. Lethaia 54, 300–313. https://doi.org/10.1111/let.12403.

Ferretti, A., Medici, L., Savioli, M., Mascia, M.T., Malferrari, D., 2021b. Dead, fossil or alive: Bioapatite diagenesis and fossilization. Palaeogeogr. Palaeoclimatol. Palaeoecol. 579, 110608 https://doi.org/10.1016/j.palaeo.2021.110608.

Ferretti, A., Corriga, M.G., Slavík, L., Corradini, C., 2022. Running across the Silurian/Devonian Boundary along Northern Gondwana: A Conodont Perspective. Geosciences 12, 43. https://doi.org/10.3390/geosciences12010043.

Ferretti, A., Schönlaub, H.P., Sachanski, V., Bagnoli, G., Serpagli, E., Vai, G.B., Yanev, S., Radonjić, M., Balica, C., Bianchini, L., Colmenar, J., Gutiérrez-Marco, J.C., 2023. A global view on the Ordovician stratigraphy of southeastern Europe. Geol. Soc. Lond. Spec. Publ. 532 (1), SP532-2022–174 https://doi.org/10.1144/SP532-2022-174.

Flügel, H., Schönlaub, H., 1972. Nachweis von tieferen Unterdevon und höheren Silur in der Rannch-Facies des Grazer Paläozoikums. Mitt Geol Gesell Wien 63, 142–148.

Girard, C., Albarède, F., 1996. Trace elements in conodont phosphates from the Frasnian/Famennian boundary. Palaeogeogr. Palaeoclimatol. Palaeoecol. 126, 195–209. https://doi.org/10.1016/S0031-0182(96)00114-9.

Grandjean, P., Cappetta, H., Michard, A., Albare'de, F., 1987. The assessment of REE patterns and $^{143}Nd/^{144}Nd$ ratios in fish remains. Earth Planet. Sci. Lett. 84, 181–196. https://doi.org/10.1016/0012-821X(87)90084-7.

Grandjean-Lécuyer, P., Feist, R., Albarède, F., 1993. Rare earth elements in old biogenic apatites. Geochim. Cosmochim. Acta 57, 2507–2514. https://doi.org/10.1016/0016-7037(93)90413-Q.
Haley, B.A., Klinkhammer, G.P., McManus, J., 2004. Rare earth elements in pore waters of marine sediments. Geochim. Cosmochim. Acta 68, 1265–1279. https://doi.org/10.1016/j.gca.2003.09.012.
Herwartz, D., Tütken, T., Jochum, K.P., Sander, P.M., 2013. Rare earth element systematics of fossil bone revealed by LA-ICPMS analysis. Geochim. Cosmochim. Acta 103, 161–183. https://doi.org/10.1016/j.gca.2012.10.038.
Holser, W.T., 1997. Evaluation of the application of rare-earth elements to paleoceanography. Palaeogeogr. Palaeoclimatol. Palaeoecol. 132, 309–323. https://doi.org/10.1016/S0031-0182(97)00069-2.
Jentzsch, I., 1962. Conodonten aus Tentaculitenknollennalk (Unterdevon) in Thüringen. Geologie 11, 961–985.
Kamber, B.S., Webb, G.E., 2001. The geochemistry of late Archaean microbial carbonate: implications for ocean chemistry and continental erosion history. Geochim. Cosmochim. Acta 65, 2509–2525. https://doi.org/10.1016/S0016-7037(01)00613-5.
Kaminski, M.A., Ferretti, A., Messori, F., Papazzoni, C.A., Sevastopulo, G., 2016. Silurian agglutinated foraminifera from the Dingle Peninsula, Ireland. Boll. Soc. Paleontol. Ital. 127–138. https://doi.org/10.4435/BSPI.2016.12.
Keenan, S.W., Engel, A.S., 2017. Early diagenesis and recrystallization of bone. Geochim. Cosmochim. Acta 196, 209–223. https://doi.org/10.1016/j.gca.2016.09.033.
Keenan, S.W., Engel, A.S., Roy, A., Lisa Bovenkamp-Langlois, G., 2015. Evaluating the consequences of diagenesis and fossilization on bioapatite lattice structure and composition. Chem. Geol. 413, 18–27. https://doi.org/10.1016/j.chemgeo.2015.08.005.
Kidder, D.L., Krishnaswamy, R., Mapes, R.H., 2003. Elemental mobility in phosphatic shales during concretion growth and implications for provenance analysis. Chem. Geol. 198, 335–353. https://doi.org/10.1016/S0009-2541(03)00036-6.
Kim, J.-M., Chung, H.-T., 2003. Electrochemical characteristics of orthorhombic $LiMnO_2$ with different degrees of stacking faults. J. Power Sources 115, 125–130. https://doi.org/10.1016/S0378-7753(02)00709-7.
Kim, J.-H., Torres, M.E., Haley, B.A., Kastner, M., Pohlman, J.W., Riedel, M., Lee, Y.-J., 2012. The effect of diagenesis and fluid migration on rare earth element distribution in pore fluids of the northern Cascadia accretionary margin. Chem. Geol. 291, 152–165. https://doi.org/10.1016/j.chemgeo.2011.10.010.
Kocsis, L., Trueman, C.N., Palmer, M.R., 2010. Protracted diagenetic alteration of REE contents in fossil bioapatites: Direct evidence from Lu–Hf isotope systematics. Geochim. Cosmochim. Acta 74, 6077–6092. https://doi.org/10.1016/j.gca.2010.08.007.
Kowal-Linka, M., Jochum, K.P., Surmik, D., 2014. LA-ICP-MS analysis of rare earth elements in marine reptile bones from the Middle Triassic bonebed (Upper Silesia, S Poland): Impact of long-lasting diagenesis, and factors controlling the uptake. Chem. Geol. 363, 213–228. https://doi.org/10.1016/j.chemgeo.2013.10.038.
Kříž, J., 1992. Silurian Field Excursions: Prague Basin (Barrandian). National Museum of Wales - Geological Series, Bohemia.
Kříž, J., 1998. Silurian. In: Chlupáč, I., Havlíček, V., Kříž, J., Kukal, Z., Štorch, P. (Eds.), Paleozoic of the Barrandian (Cambrian to Devonian). Prague,, pp. 79–101.
Kříž, J., Jaeger, H., Paris, F., Schönlaub, H.P., 1986. Přídolí – the fourth Subdivision of the Silurian. Jb. Geol. B.-A. 129, 291–360.
Kříž, J., Degarding, J., Ferretti, A., Hansch, W., Gutierrez-Marco, J., Paris, F., Picarra de Almeida, J., Robardet, M., Schönlaub, H.P, Serpagli, E., 2003. Silurian stratigraphy and paleogeography of Gondwanan and Perunican Europe. In: Landing, E., Johnson, M.E. (Eds.), Silurian Lands and Seas – Paleogeography outside Laurentia. New York State Museum Bulletin, pp. 105–178.
Lécuyer, C., Reynard, B., Grandjean, P., 2004. Rare earth element evolution of Phanerozoic seawater recorded in biogenic apatites. Chem. Geol. 204, 63–102. https://doi.org/10.1016/j.chemgeo.2003.11.003.
Lehnert, O., Frýda, J., Buggisch, W., Munnecke, A., Nützel, A., Kříž, J., Manda, S., 2007. $\delta^{13}C$ records across the late Silurian Lau event: New data from middle palaeolatitudes of northern peri-Gondwana (Prague Basin, Czech Republic). Palaeogeogr. Palaeoclimatol. Palaeoecol. 245, 227–244. https://doi.org/10.1016/j.palaeo.2006.02.022.
Lešer, V., Milani, M., Tatti, F., Pipan Tkalec, Ž., Štrus, J., Drobne, D., 2010. Focused ion beam (FIB)/scanning electron microscopy (SEM) in tissue structural research. Protoplasma 246, 41–48. https://doi.org/10.1007/s00709-010-0118-8.
Li, Y., Zhao, L., Chen, Z.-Q., Algeo, T.J., Cao, L., Wang, X., 2017. Oceanic environmental changes on a shallow carbonate platform (Yangou, Jiangxi Province, South China) during the Permian-Triassic transition: evidence from rare earth elements in conodont bioapatite. Palaeogeogr. Palaeoclimatol. Palaeoecol. 486, 6–16. https://doi.org/10.1016/j.palaeo.2017.02.035.
Liao, J., Sun, X., Li, D., Sa, R., Lu, Y., Lin, Z., Xu, L., Zhan, R., Pan, Y., Xu, H., 2019. New insights into nanostructure and geochemistry of bioapatite in REE-rich deep-sea sediments: LA-ICP-MS, TEM, and Z-contrast imaging studies. Chem. Geol. 512, 58–68. https://doi.org/10.1016/j.chemgeo.2019.02.039.
Liu, Y.-G., Miah, M.R.U., Schmitt, R.A., 1988. Cerium: a chemical tracer for paleo-oceanic redox conditions. Geochim. Cosmochim. Acta 52, 1361–1371. https://doi.org/10.1016/0016-7037(88)90207-4.
Malferrari, D., Ferretti, A., Mascia, M.T., Savioli, M., Medici, L., 2019. How much can we Trust Major Element Quantification in Bioapatite Investigation? ACS Omega 4, 17814–17822. https://doi.org/10.1021/acsomega.9b02426.
Manda, Š., Kříž, J., 2006. Environmental and biotic changes in subtropical isolated carbonate platforms during the late Silurian Kozlowskii Event, Prague Basin. GFF 128, 161–168. https://doi.org/10.1080/11035890601282161.
Manda, Š., Slavík, L., Štorch, P., Tasáryová, Z., Čáp, P., 2023. Division of Přídolí Series in Central Bohemia: graptolite and conodont biostratigraphy, faunal changes, and geochemical record. Newsl. Stratigr. 56, 89–123. https://doi.org/10.1127/nos/2022/0695.
McLennan, S.M., 2001. Relationships between the trace element composition of sedimentary rocks and upper continental crust: trace element composition and upper continental crust. Geochem. Geophys. Geosystems 2. https://doi.org/10.1029/2000GC000109.
Medici, L., Malferrari, D., Savioli, M., Ferretti, A., 2020. Mineralogy and crystallization patterns in conodont bioapatite from first occurrence (Cambrian) to extinction (end-Triassic). Palaeogeogr. Palaeoclimatol. Palaeoecol. 549 https://doi.org/10.1016/j.palaeo.2019.02.024.
Medici, L., Savioli, M., Ferretti, A., Malferrari, D., 2021. Zooming in REE and other trace elements on conodonts: does taxonomy guide diagenesis? J. Earth Sci. https://doi.org/10.1007/s12583-020-1094-3.
Mergl, M., 2019. Problematic sclerites *Eurytholia* from the Lower and Middle Devonian of the Czech Republic. Folia Musei Rerum Nat. Bohem. Occident. Geol. Paleobiologica 53, 1–11. https://doi.org/10.2478/fbgp-2019-0001.
Möstler, H., 1968. Das Silur im Westabschnitt der Nördlichen Grauwackenzone (Tirol und Salzburg). Mitt. Ges. Geol. Bergbaustud. 18, 89–150.
Nardelli, M.P., Malferrari, D., Ferretti, A., Bartolini, A., Sabbatini, A., Negri, A., 2016. Zinc incorporation in the miliolid foraminifer *Pseudotriloculina rotunda* under laboratory conditions. Mar. Micropaleontol. 126, 42–49. https://doi.org/10.1016/j.marmicro.2016.06.001.
Nothdurft, L.D., Webb, G.E., Kamber, B.S., 2004. Rare earth element geochemistry of Late Devonian reefal carbonates, Canning Basin, Western Australia: confirmation of a seawater REE proxy in ancient limestones. Geochim. Cosmochim. Acta 68, 263–283. https://doi.org/10.1016/S0016-7037(03)00422-8.
Nozaki, Y., Zhang, J., Amakawa, H., 1997. The fractionation between Y and Ho in the marine environment. Earth Planet. Sci. Lett. 148, 329–340. https://doi.org/10.1016/S0012-821X(97)00034-4.
Pattan, J.N., Pearce, N.J.G., Mislankar, P.G., 2005. Constraints in using Cerium-anomaly of bulk sediments as an indicator of paleo bottom water redox environment: a case study from the Central Indian Ocean Basin. Chem. Geol. 221, 260–278. https://doi.org/10.1016/j.chemgeo.2005.06.009.
Peppe, D.J., Reiners, P.W., 2007. Conodont (U–Th)/He thermochronology: initial results, potential, and problems. Earth Planet. Sci. Lett. 258, 569–580. https://doi.org/10.1016/j.epsl.2007.04.022.
Picard, S., Lécuyer, C., Barrat, J.-A., Garcia, J.-P., Dromart, G., Sheppard, S.M.F., 2002. Rare earth element contents of Jurassic fish and reptile teeth and their potential relation to seawater composition (Anglo-Paris Basin, France and England). Chem. Geol. 186, 1–16. https://doi.org/10.1016/S0009-2541(01)00424-7.
Prakash, S., Mahesh, C., Gairola, R.M., 2012. Sea level anomalies in the tropical Indian Ocean during two contrasting southwest monsoon years. Int. J. Ocean Clim. Syst. 3, 127–133. https://doi.org/10.1260/1759-3131.3.2.127.
Pucéat, E., Reynard, B., Lécuyer, C., 2004. Can crystallinity be used to determine the degree of chemical alteration of biogenic apatites? Chem. Geol. 205, 83–97. https://doi.org/10.1016/j.chemgeo.2003.12.014.
Reynard, B., Lécuyer, C., Grandjean, P., 1999. Crystal-chemical controls on rare-earth element concentrations in fossil biogenic apatites and implications for paleoenvironmental reconstructions. Chem. Geol. 155, 233–241. https://doi.org/10.1016/S0009-2541(98)00169-7.
Rosseeva, E., Borrmann, H., Cardoso-Gil, R., Carrillo-Cabrera, W., Frank-Kamenetskaya, O., Öztan, Y., Prots, Y., Schwarz, U., Simon, P., Zhuravlev, A., Kniep, Z., 2011. Evolution and complexity of dental (apatite-based) biominerals: mimicking the very beginning in the laboratory. Max-Planck-Institut für Chemische Physik fester Stoffe, Scientific Report 2009–2010.
Sansom, I., 1996. *Pseudooneotodus*: a histological study of an Ordovician to Devonian vertebrate lineage. Zool. J. Linnean Soc. 118, 47–57.
Schönlaub, H., 1997. The Silurian of Austria. Jb. Geol. B.-A. 40, 20–41.
Schönlaub, H.P., Corradini, C., Corriga, M.G., Ferretti, A., 2017. Chrono-, litho- and conodont bio-stratigraphy of the Rauchkofel Boden Section (Upper Ordovician – lower Devonian), Carnic Alps. Austria, Newsl. Stratigr. 50, 445–469. https://doi.org/10.1127/nos/2017/0391.
Schulze, R., 1968. Die Conodonten aus dem Paläozoikum der mittleren Karawanken Seeberggebiet. N. Jb. Geol. Palaont. 130, 133–245.
Scotese, C., 2014. Atlas of Silurian and Middle-Late Ordovician Paleogeographic Maps (Mollweide Projection). In: Maps 73–80. PALEOMAP Atlas for ArcGIS, 5. PALEOMAP Project.
Serpagli, E., 1970. Uppermost Wenlockian-Upper Ludlowian (Silurian) Conodonts from Western Sardinia. Boll. Soc. Paleontol. Ital. 9, 76–96.
Serpagli, E., Corradini, C., Ferretti, A., 1998. Conodonts from a Ludlow-Pridoli section near the Silius village. Giorn. Geologia 60, 104–111.
Shen, J., Algeo, T.J., Zhou, L., Feng, Q., Yu, J., Ellwood, B., 2012. Volcanic perturbations of the marine environment in South China preceding the latest Permian mass extinction and their biotic effects. Geobiology 10, 82–103. https://doi.org/10.1111/j.1472-4669.2011.00306.x.
Sholkovitz, E., Shen, G.T., 1995. The incorporation of rare earth elements in modern coral. Geochim. Cosmochim. Acta 59, 2749–2756. https://doi.org/10.1016/0016-7037(95)00170-5.
Skinner, H.C.W., 2005. Biominerals. Mineral. Mag. 69, 621–641. https://doi.org/10.1180/0026461056950275.
Slavík, L., 2017. Conodonts from the Silurian and Devonian of the Požáry Quarries. Ber. Inst. Erdwiss. K-F-Univ. Graz 23, 139–152.
Slavík, L., Hladil, J., 2017. Geological overview of the Paleozoic of the Barrandian Unit. Ber. Inst. Erdwiss. K-F-Univ. Graz 23, 129–134.

Soyol-Erdene, T.-O., Huh, Y., 2013. Rare earth element cycling in the pore waters of the Bering Sea Slope (IODP Exp. 323). Chem. Geol. 358, 75–89. https://doi.org/10.1016/j.chemgeo.2013.08.047.
Stouge, S., 1984. Conodonts of the Middle Ordovician Table Head Formation, western Newfoundland. Foss. Strat. 16, 1–145.
Sutton, M.D., Holmer, L.E., Cherns, L., 2001. Small problematic phosphatic sclerites from the Ordovician of Iapetus. J. Paleontol. 75, 1–8. https://doi.org/10.1666/0022-3360(2001)075<0001:SPPSFT>2.0.CO;2.
Taylor, S.R., McLennan, S.M., 1985. The Continental Crust: Its Composition and Evolution. Blackwell Scientific Pub, Palo Alto, CA.
Toyoda, K., Tokonami, M., 1990. Diffusion of rare-earth elements in fish teeth from deep-sea sediments. Nature 345, 607–609. https://doi.org/10.1038/345607a0.
Trotter, J.A., Eggins, S.M., 2006. Chemical systematics of conodont apatite determined by laser ablation ICPMS. Chem. Geol. 233, 196–216. https://doi.org/10.1016/j.chemgeo.2006.03.004.
Trotter, J.A., Gerald, J.D.F., Kokkonen, H., Barnes, C.R., 2007. New insights into the ultrastructure, permeability, and integrity of conodont apatite determined by transmission electron microscopy. Lethaia 40, 97–110. https://doi.org/10.1111/j.1502-3931.2007.00024.x.
Trotter, J.A., Barnes, C.R., McCracken, A.D., 2016. Rare earth elements in conodont apatite: Seawater or pore-water signatures? Palaeogeogr. Palaeoclimatol. Palaeoecol. 462, 92–100. https://doi.org/10.1016/j.palaeo.2016.09.007.
Trueman, C.N., Tuross, N., 2002. Trace elements in recent and Fossil Bone Apatite. Rev. Mineral. Geochem. 48, 489–521. https://doi.org/10.2138/rmg.2002.48.13.
Trueman, C.N., Privat, K., Field, J., 2008. Why do crystallinity values fail to predict the extent of diagenetic alteration of bone mineral? Palaeogeogr. Palaeoclimatol. Palaeoecol. 266, 160–167. https://doi.org/10.1016/j.palaeo.2008.03.038.
Tung, H.-M., Huang, J.-H., Tsai, D.-G., Ai, C.-F., Yu, G.-P., 2009. Hardness and residual stress in nanocrystalline ZrN films: effect of bias voltage and heat treatment. Mater. Sci. Eng. A 500, 104–108. https://doi.org/10.1016/j.msea.2008.09.006.
Turner, S., Burrow, C.J., Schultze, H.-P., Blieck, A., Reif, W.-E., Rexroad, C.B., Bultynck, P., Nowlan, G.S., 2010. False teeth: conodont-vertebrate phylogenetic relationships revisited. Geodiversitas 32, 545–594. https://doi.org/10.5252/g2010n4a1.
von Raumer, J.F., Stampfli, G.M., 2008. The birth of the Rheic Ocean — early Palaeozoic subsidence patterns and subsequent tectonic plate scenarios. Tectonophysics 461, 9–20. https://doi.org/10.1016/j.tecto.2008.04.012.
Walliser, O., 1964. Conodonten des Silurs. Abh. Hess. L.-Amt Bodenforsch 41, 1–106.
Webb, G.E., Kamber, B.S., 2000. Rare earth elements in Holocene reefal microbialites: a new shallow seawater proxy. Geochim. Cosmochim. Acta 64, 1557–1565. https://doi.org/10.1016/S0016-7037(99)00400-7.
Webb, G.E., Nothdurft, L.D., Kamber, B.S., Kloprogge, J.T., Zhao, J.-X., 2009. Rare earth element geochemistry of scleractinian coral skeleton during meteoric diagenesis: a sequence through neomorphism of aragonite to calcite. Sedimentology 56, 1433–1463. https://doi.org/10.1111/j.1365-3091.2008.01041.x.
Winder, C., 1976. Enigmatic objects in North America Ordovician carbonates. In: Bassett, M. (Ed.), The Ordovician System: Proceedings of a Palaeontological Association Symposium, Birmingham, September 1974. Presented at the the Ordovician System. University of Wales Press and the National Museum of Wales for the Palaeontological Association, Cardiff.
Wright, J., Colling, A., 1995. Seawater: Its Composition, Properties, and Behaviour, Second. ed. Pergamon Press, in association with the Open University, Oxford, pp. 85-127.
Wright, J., Seymour, R.S., Shaw, H.F., 1984. In: REE and Nd isotopes in conodont apatite: Variations with geological age and depositional environment. Clark, L.D. (Ed), Conodont Biofacies and Provincialism. Geological Society of America 196 (Special Papers), pp. 325–340. https://doi.org/10.1130/SPE196-p325.
Wright, J., Schrader, H., Holser, W.T., 1987. Paleoredox variations in ancient oceans recorded by rare earth elements in fossil apatite. Geochim. Cosmochim. Acta 51, 631–644. https://doi.org/10.1016/0016-7037(87)90075-5.
Zapanta LeGeros, R., 1981. Apatites in biological systems. Prog. Cryst. Growth Charact. 4, 1–45. https://doi.org/10.1016/0146-3535(81)90046-0.
Zhang, J., Nozaki, Y., 1996. Rare earth elements and yttrium in seawater: ICP-MS determinations in the East Caroline, Coral Sea, and South Fiji basins of the western South Pacific Ocean. Geochim. Cosmochim. Acta 60, 4631–4644. https://doi.org/10.1016/S0016-7037(96)00276-1.
Zhang, K., Shields, G.A., 2022. Sedimentary Ce anomalies: Secular change and implications for paleoenvironmental evolution. Earth-Sci. Rev. 229, 104015 https://doi.org/10.1016/j.earscirev.2022.104015.
Zhang, J., Amakawa, H., Nozaki, Y., 1994. The comparative behaviors of yttrium and lanthanides in the seawater of the North Pacific. Geophys. Res. Lett. 21, 2677–2680. https://doi.org/10.1029/94GL02404.
Zhang, L., Algeo, T.J., Cao, L., Zhao, L., Chen, Z.-Q., Li, Z., 2016. Diagenetic uptake of rare earth elements by conodont apatite. Palaeogeogr. Palaeoclimatol. Palaeoecol. 458, 176–197. https://doi.org/10.1016/j.palaeo.2015.10.049.
Zhao, L., Chen, Z.-Q., Algeo, T.J., Chen, J., Chen, Y., Tong, J., Gao, S., Zhou, L., Hu, Z., Liu, Y., 2013. Rare-earth element patterns in conodont albid crowns: evidence for massive inputs of volcanic ash during the latest Permian biocrisis? Glob. Planet. Change 105, 135–151. https://doi.org/10.1016/j.gloplacha.2012.09.001.
Zhuravlev, A.V., Gerasimova, A.I., 2015. Albid tissue of the conodont elements: composition and forming model. Vestn. Inst. Geol. Komi Sci. Cent. Ural Branch RAS 2015, 21–27. https://doi.org/10.19110/2221-1381-2015-10-21-27.
Žigaitė, Ž., Qvarnström, M., Bancroft, A., Pérez-Huerta, A., Blom, H., Ahlberg, P.E., 2020. Trace and rare earth element compositions of Silurian conodonts from the Vesiku Bone Bed: Histological and palaeoenvironmental implications. Palaeogeogr. Palaeoclimatol. Palaeoecol. 549, 109449 https://doi.org/10.1016/j.palaeo.2019.109449.